Dalton Transactions

The pathway for serial proton supply to the active site of nitrogenase: enhanced density functional modeling of the Grotthuss mechanism

Journal:	*Dalton Transactions*
Manuscript ID	DT-ART-08-2015-003223.R1
Article Type:	Paper
Date Submitted by the Author:	21-Sep-2015
Complete List of Authors:	Dance, Ian; UNSW Australia, Chemistry

SCHOLARONE™
Manuscripts

The pathway for serial proton supply to the active site of nitrogenase: enhanced density functional modeling of the Grotthuss mechanism

Ian Dance

School of Chemistry, UNSW Australia, Sydney 2052, Australia

Abstract

Nitrogenase contains a well defined and conserved chain of water molecules leading to the FeMo cofactor (FeMo-co, an $[Fe_7MoCS_9]$ cluster with bidentate chelation of Mo by homocitrate) that is the active site where N_2 and other substrates are sequentially hydrogenated using multiple protons and electrons. The function of this chain is proposed to be a proton wire, serially translocating protons to triply-bridging S3B of FeMo-co, where, concomitant with electron transfer to FeMo-co, an H atom is generated on S3B. Density functional simulations of this proton translocation mechanism are reported here, using a large 269-atom model that includes all residues hydrogen bonded to and surrounding the water chain, and likely to influence proton transfer: three carboxylate O atoms of obligatory homocitrate are essential. The mechanism involves the standard two components of the Grotthuss mechanism, namely H atom slides that shift H_3O^+ from one water site to the next, and HOH molecular rotations that convert backward (posterior) OH bonds in the water chain to forward (anterior) OH bonds. The topography of the potential energy surface for each of these steps has been mapped. H atom slides pass through very short (ca 2.5Å) O-H-O hydrogen bonds, while HOH rotations involve the breaking of O-H•••O hydrogen bonds, and the occurrence of long (up to 3.6Å) separations between contiguous water molecules. Both steps involve low potential energy barriers, < 7 kcal mol^{-1}. During operation of the Grotthuss mechanism in nitrogenase there are substantial displacements of water molecules along the chain, occurring as ripples when concerted. These characteristics of the 'Grotthuss two-step', coupled with a buffering ability of two carboxylate O atoms of homocitrate, and combined with density functional characterisation of the final proton slide from the ultimate water molecule to S3B (including electron addition), have been choreographed into a complete mechanism for serial hydrogenation of FeMo-co. The largest potential barrier is estimated to be 14 kcal mol^{-1}. These results are discussed in the context of reactivity data for nitrogenase, and the occurrence of a comparable water chain in cytochrome-c oxidase. Further investigation of the low-frequency conformational dynamics of the nitrogenase proteins, coupling proton transfer with other events in the nitrogenase cycle, is briefly canvassed.

Introduction

The enzyme nitrogenase catalyses the reaction $N_2 + 6e^- + 6H^+ \rightarrow 2NH_3$, together with some reduction of protons to H_2.[1-9] Nitrogenase can also hydrogenate many other small multiply-bonded molecules, including CO and CO_2.[3,10-16] A distinctive feature of these reactions is the consumption of considerable numbers of protons (and equivalent electrons) during each catalytic cycle. The natural cycle of nitrogenase, involving co-reduction of N_2 and H^+, requires *ca* $8H^+$, while the observed conversion of CO to C_3H_8 presumably follows an overall stoichiometry $3CO + 14e^- + 14H^+$, requiring 14 protons per cycle. Obviously the enzyme requires a serial supply of protons, and most if not all of these must be sourced from the medium outside the protein.

I previously identified a chain of water molecules that extends from the protein surface to the active site, and proposed in general terms how a Grotthuss type of proton translocation along this chain could be the mechanism for serial proton provision.[17] This water channel was first recognised by Durrant,[18] and has been discussed also by Barney *et al.*[19] In the present paper I report a more detailed investigation of this mechanism for serial translocation of protons to the active site, using density functional simulations of models that include the protein residues surrounding the water chain.

The active site is the FeMo-cofactor (FeMo-co) located in the α subunit of the molybdenum-iron protein (MoFe protein). The biochemical events in the Fe protein cycle, in which the other protein comprising nitrogenase, the Fe protein, docks with the MoFe protein and subsequently transfers an electron to FeMo-co, via a P-cluster in the MoFe protein, have been described in detail.[3,20,5-8] The structure of FeMo-co is shown in Fig 1. The central Fe_7MoS_9 cluster contains a carbon atom C^c at the centre,[21-23] and is connected to protein through 275^{Cys} at Fe1 and 442^{His} at Mo: amino acid numbering is that of the *Azotobacter vinelandii* protein as reported in the crystal structures PDB 1M1N and 3U7Q. Throughout this paper all cited residues are in the α-subunit unless marked otherwise. Six-coordinate Mo is chelated by alcoxide and carboxylate functions of *R*-homocitrate (*R*-2-hydroxybutane-1,2,4-tricarboxylate), abbreviated as hca hereafter.

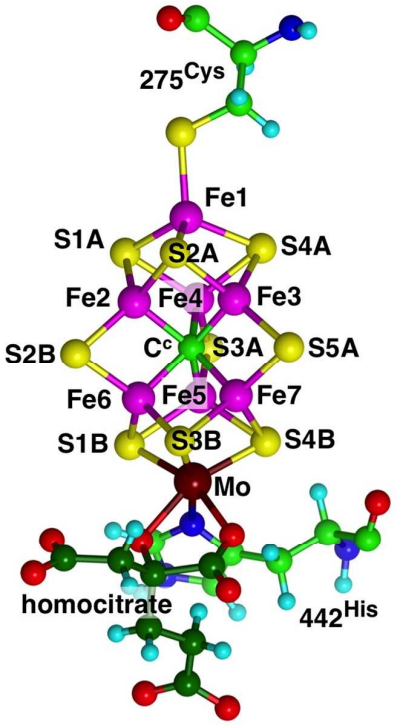

Fig 1. FeMo-co, linked to protein via 275^{Cys} at Fe1 and 442^{His} at Mo. Atom labels are those of the *Azotobacter vinelandii* protein. Carbon atoms of bidentate homocitrate are dark green.

1. The water chain of nitrogenase

The essential water molecules comprising the water chain are shown in Fig 2. Moving outward from the triply-bridging S atom S3B of FeMo-co there is a completely conserved sequence of eight water molecules, W1 to W8, hydrogen bonded in sequence as well as to surrounds. This chain is denoted the proton wire, because it is the key focus for proton movement towards FeMo-co. Continuing towards the protein surface, there is a domain containing variable arrangements of hydrogen bonded water molecules, and in some crystal structures containing also exogenous hydrophilic molecules such as ethylene glycol and imidazolium cation arising from the crystallisation medium.[17,24] This domain is interpreted as a proton bay, because it has variable ways of including water, H_3O^+, and exogenous proton sources. The section of the water chain that is under strict mechanistic control, the proton wire W1 to W8, is therefore the focus of the following analyses. Additional pictorial presentations of the water chain within the larger protein structure are available in ref [17], and also ref [24]. The water chain is well separated from the probable pathway for ingress of substrate N_2 (and other uncharged small molecules) to FeMo-co,[24] and from the pathway proposed for egress of the hydrophilic product NH_3.[25]

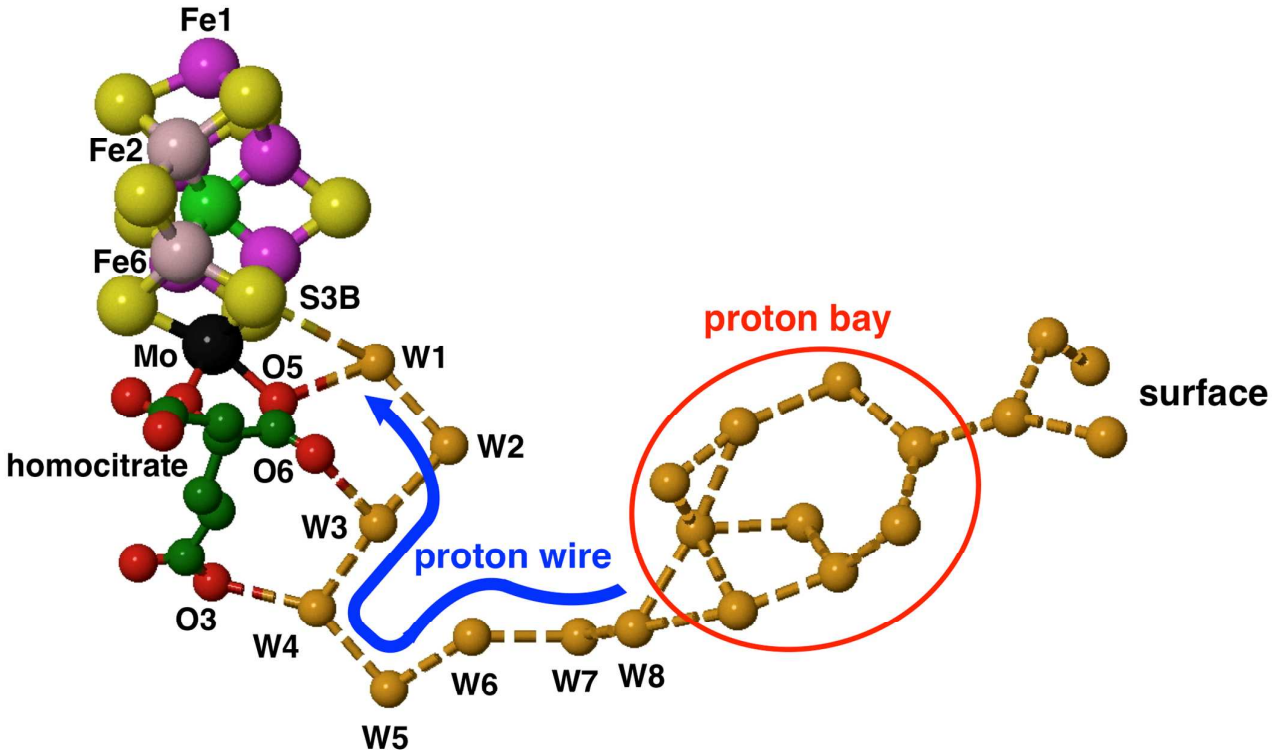

Fig 2. Interpretation of the water chain, with an aggregated proton bay inside the surface, followed by the proton wire from W8 to S3B.

This path is elaborated in Fig 3 (a), aided by schematic representation in Fig 3 (b). The key hydrogen bonds, apart from those along the chain, are W1--O5(hca), main-chain NH of 97^{Arg} to W2, W3--O6(hca), W3--CO of 95^{Gly}, W4--O3(hca), side-chain NH_2 of β-105^{Arg} to W4, side-chain Nε of β-105^{Arg} to W5, W5--OH of 446^{Tyr}, W6--CO of 95^{Gly}, W7--CO of δ-522^{Val}, W8--CO of 94^{Ala}, and main-chain NH of δ-521^{Leu} to W2. In addition, W1 is able to hydrogen bond with main-chain CO of 442^{His}. A significant feature of the carbonyl O of 95^{Gly} is its linkage of the W3 and W6 ends of a loop in the water chain. Also marked on Fig 3 (a) are the hydrogen bonds between the residues included, and the structural hydrogen bond between S5A of FeMo-co and the side-chain of 96^{Arg}.

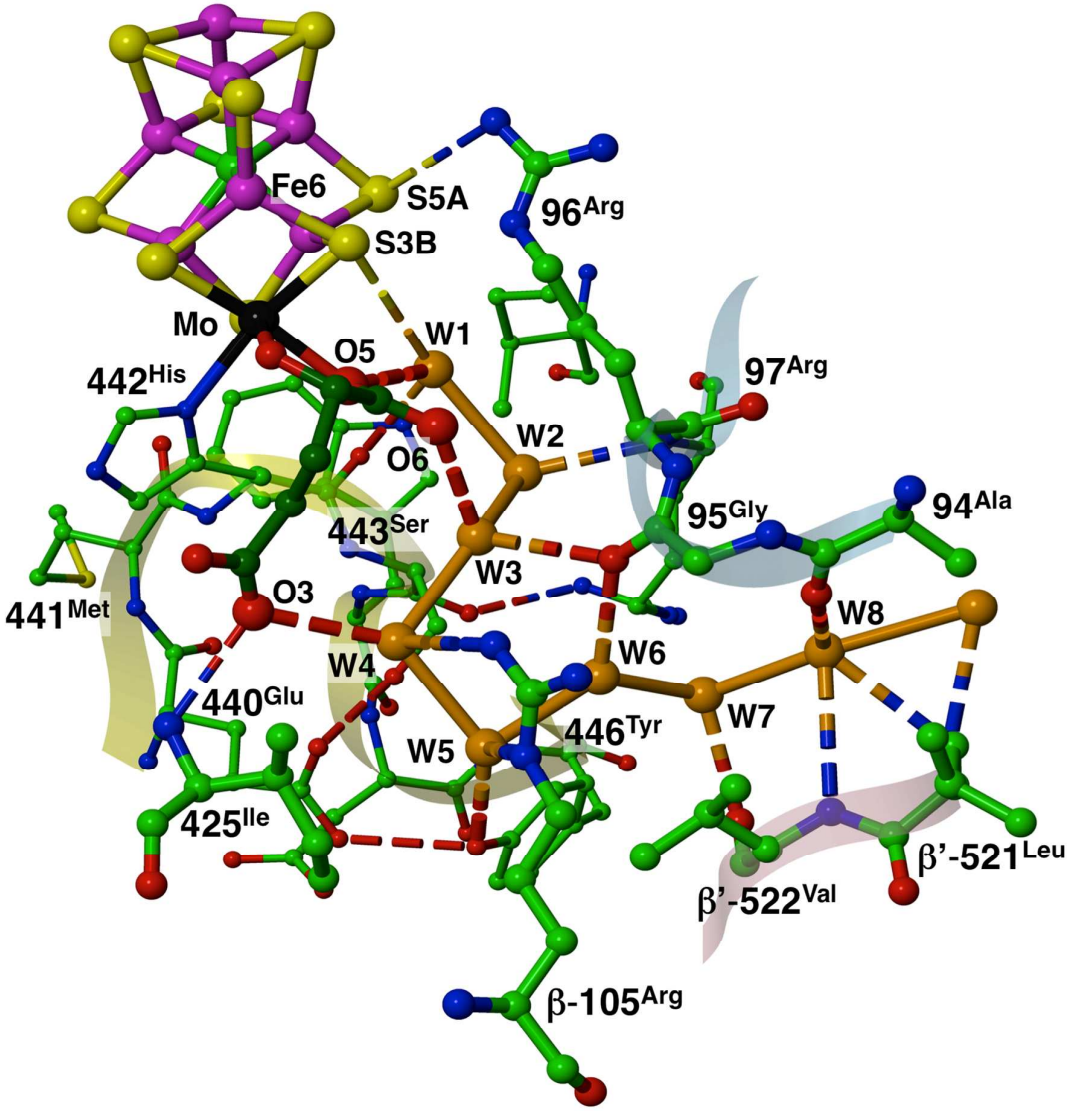
Fe6
S5A
96Arg
S3B
Mo
O5
W1
442His
97Arg
O6
W2
95Gly
94Ala
443Ser
W3
O3
441Met
W8
W6
W4
440Glu
446Tyr
W7
W5
425Ile
β'-521Leu
β'-522Val
β-105Arg

(a)

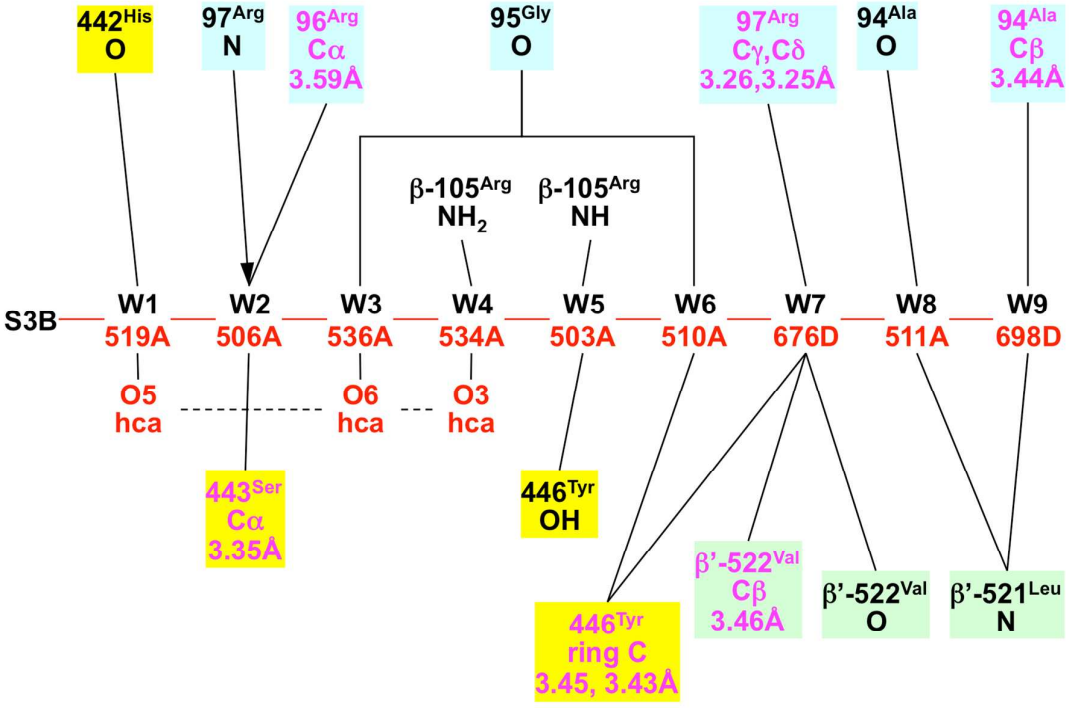
442His O
97Arg N
96Arg Cα 3.59Å
95Gly O
97Arg Cγ,Cδ 3.26,3.25Å
94Ala O
94Ala Cβ 3.44Å
β-105Arg NH2
β-105Arg NH
S3B
W1 519A
W2 506A
W3 536A
W4 534A
W5 503A
W6 510A
W7 676D
W8 511A
W9 698D
O5 hca
O6 hca
O3 hca
443Ser Cα 3.35Å
446Tyr OH
β'-522Val Cβ 3.46Å
β'-522Val O
β'-521Leu N
446Tyr ring C 3.45, 3.43Å

(b)

Fig 3. Details of the water path from W8 to S3B of FeMo-co. (a) The chain of hydrogen bonded water molecules is coloured orange. The C atoms of hca (irrelevant carboxylate arm not shown) are dark green: O5, O6 and O3 of hca are labelled and the water--hca hydrogen bonds W1--O5, W3--O6 and W4--O3 are coloured red. Other hydrogen bonds involving the water chain are thicker, and residues to the front are drawn with larger atoms and bonds than those behind. All residues are in the α-chain except for β-105^{Arg}, β'-521^{Leu} and β'-522^{Val}, and the ribbons trace the three chain sections surrounding the water path. (b) Schematic representation of the water path, with water labels for one of the paths in crystal 3U7Q. Hydrogen bonds with surrounding residues are marked with black lines, and C-H → O interactions are labeled in magenta, with marked C--O distances.

Also in the surrounds of the water chain are some residues that provide van der Waals enclosure, potentially restricting movement of the water molecules. These are shown in Fig 4, and some distances are marked on Fig 3 (b). The long interaction between ring Cε1 of 446^{Tyr} and W6 is discussed further below.

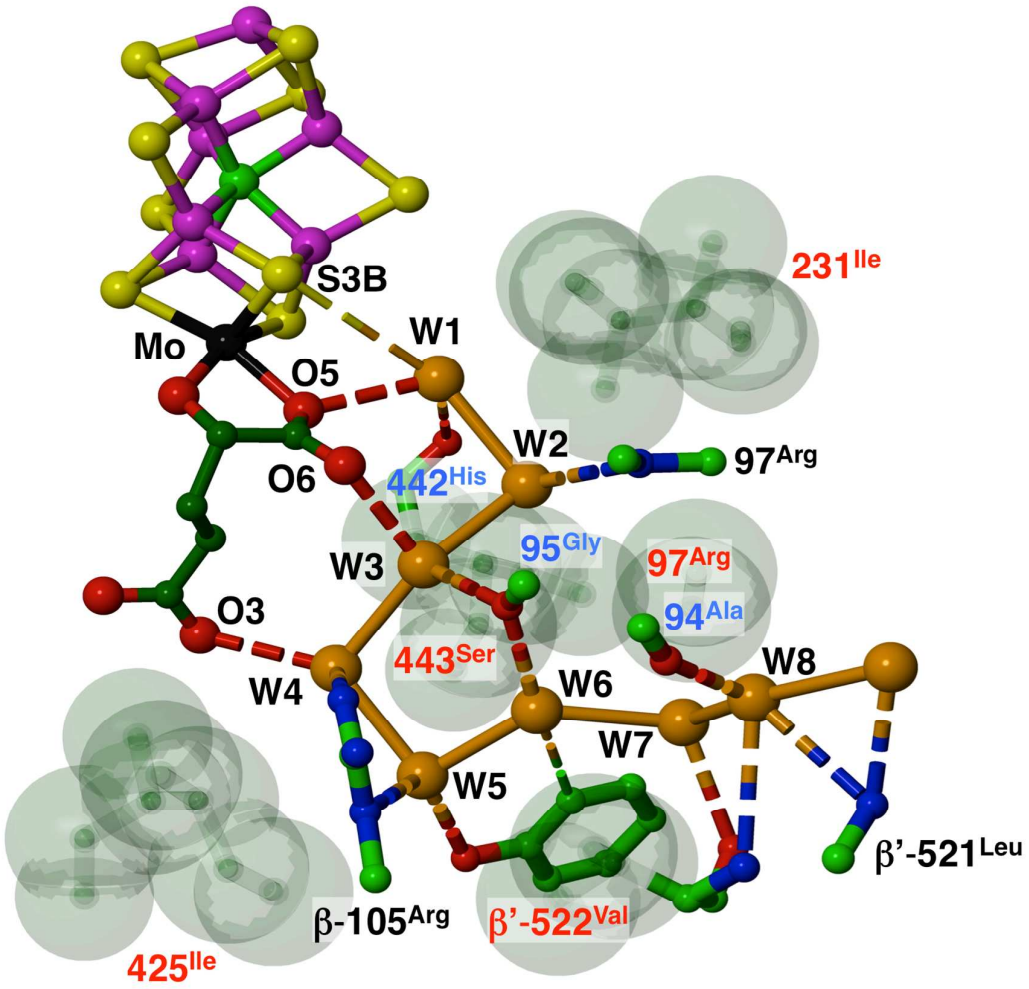

Fig 4. Residues comprising the van der Waals enclosure of the water chain to W8 are drawn as translucent green surfaces, and labelled red. The three main-chain CO groups involved in the chain are labelled blue. The uninvolved arm of hca is not shown.

2. Hydrogen atom locations and hydrogen bonding

The locations of hydrogen atoms on the water molecules, hca, and residue side-chains are not evident in the diffraction analyses. I now describe the water chain within its surroundings in order to assess the

possible positions of these hydrogen atoms and of hydrogen bonding. The surroundings are considered first, with reference to Fig 5. The side-chains of 96^{Arg} and β-105^{Arg} are protonated. That of 96^{Arg} hydrogen bonds to S5A of FeMo-co, and the side-chain of β-105^{Arg} donates hydrogen bonds to W4 and W5: to W4 from its NH_2 terminus, and to W5 from Nε. The uncoordinated carboxylic functions of homocitrate are protonated. At the O3/O4 carboxylate, O4 is hydrogen bonded to a small pool of water molecules (bounded by 426^{Lys}, 424^{Gly}, β-101^{Ser}), and in PDB 3U7Q and PDB 4WES forms good tetrahedrally-arrayed hydrogen bonds with three water molecules: this small water pool (not shown in Fig 5) has been described previously.[17,25] O3 receives a hydrogen bond from NH of 425^{Ile}, and is able to accept a hydrogen bond from W4. The O5/O6 carboxylate group is coordinated to Mo, reducing its basicity, and variable protonation is anticipated.

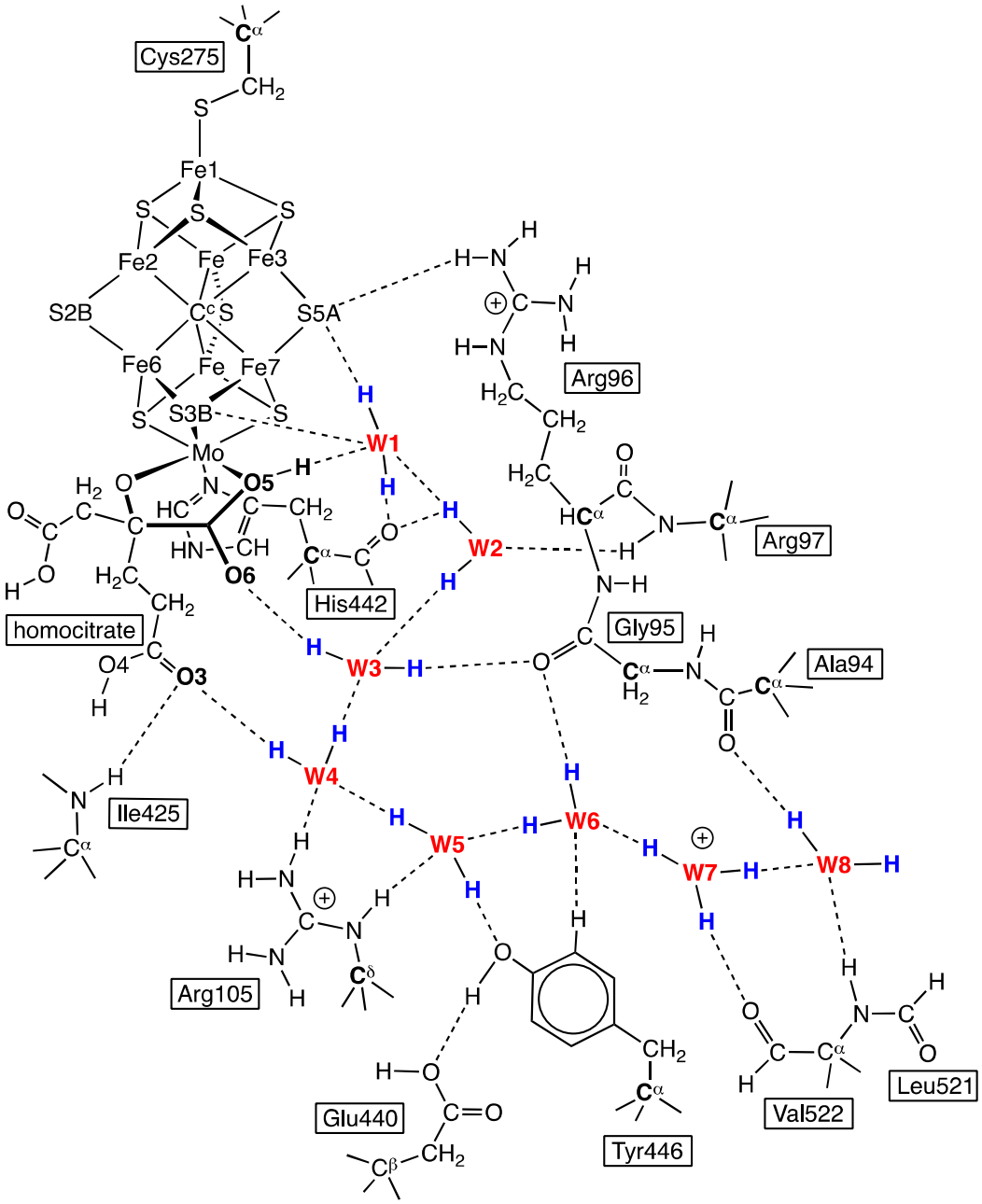

Fig 5. The relevant immediate surroundings of the water chain (red), with feasible hydrogen bonds (broken lines). Possible locations for the water hydrogen atoms are marked blue, with W7 as H_3O^+. Arg105 is β chain, and Leu521, Val522 are β' chain.

Now I consider the water molecules in the chain. The geometrical data for the potential hydrogen bonding of each are detailed in Table 1, and, again with reference to Fig 5, are analysed in terms of

possible H atom positions. There is excellent geometry at W2, which receives a good hydrogen bond from NH of 97^{Arg}. The two H atoms comprising W2 could be favourably directed to W1 and W3, because the fourth tetrahedral position around W2 is sheathed by various HC sections of 231^{Ile} and 443^{Ser}. There is space for movement of W2, and CO of 442^{His} is a potential acceptor. W1 receives one hydrogen bond from W2, and is ideally placed to hydrogen bond with O5 of homocitrate (note the ideal W2-W1-O5 geometry) as receiver or donor. The CO of 442^{His} can accept a hydrogen bond from W1, and S3B and S5A are also potential hydrogen bond acceptors from W1, with better geometry for S5A.

W3 is surrounded with good tetrahedral geometry by W2, W4, CO of 95^{Gly}, and O6, and is expected to direct a hydrogen atoms towards CO (95^{Gly}): W3 could direct another hydrogen atom to W2, W4 or O6, and could receive hydrogen bonds from any of them. W3 has multiple possibilities. W4 and W5 both receive hydrogen bonds from the positively charged side-chain of β-105^{Arg}, and both are able donate one hydrogen bond, to O3 (hca) or OH of 446^{Tyr}: the second hydrogen atoms on W4 and W5 can, with variations, be involved in the W3-W4-W5-W6 water chain. W6 donates one hydrogen bond to CO (95^{Gly}), and the other H atom can be directed to W5 or W7. A phenyl C-H atom of 446^{Tyr} is directed towards W6, but the distance and angles are relatively poor for a C-H--W6 weak hydrogen bond. In the absence of this C-H--W6 interaction, W6 is involved in only three good hydrogen bonds, unlike W3, W4, and W5, which have four. W7 also engages only three hydrogen bonds with excellent geometry, involving donation to CO (β'-522^{Val}), and sharing other H atoms with W6 and W8. At W8 the W7-W8-W9 angle is 156, reflecting the connection of the water chain to the proton bay where there is fluidity in the occurrences and positions of water molecules: W8 receives and donates hydrogen bonds to NH (β'-521^{Leu}) and CO (94^{Ala}) respectively.

Table 1. Distances (Å) and angles for the possible hydrogen bonds at each of the water molecules in the water chain, W1 to W8, in the α, β and β' subunits of PDB 3U7Q.

at **W1**	W2 donor	O5 (hca)	CO (442^{His}) acceptor	S3B acceptor	S5A acceptor
distance	2.83	2.81	3.28	4.05	4.03
W2		109°	78°	142°	154°
O5 (hca)			103°	47°	98°
CO (442^{His})				130°	105°
S3B					56°

at **W2**	W1	W3	NH (97^{Arg}) donor	CO (442^{His}) acceptor
distance	2.83	2.82	2.88	3.84
W1		95°	114°	57
W3			110°	32
NH (97^{Arg})				148

at **W3**	W2	W4	O6 (hca)	CO (95^{Gly}) acceptor
distance	2.82	2.80	2.73	2.82

W2		144°	95°	94°
W4			109°	105°
O6 (hca)				102°
at **W4**	W3	W5	O3 (hca)	NH_2 (β-105^{Arg}) donor
distance	2.80	2.79	2.87	2.94
W3		104°	115°	85°
W5			141°	73°
O3 (hca)				113°
at **W5**	W4	W6	Nε (β-105^{Arg}) donor	OH (446^{Tyr}) acceptor
distance	2.79	2.73	2.97	2.67
W4		96°	93°	132°
W6			95°	109°
Nε (β-105^{Arg})				125°
at **W6**	W5	W7	CO (95^{Gly}) acceptor	Cε1(446^{Tyr}) donor?
distance	2.73	2.83	2.73	3.45
W5		134°	115°	67°
W7			111°	69°
CO (95^{Gly})				162°
at **W7**	W6	W8	CO (β'-522^{Val}) acceptor	
distance	2.83	2.73	2.86	
W6		107°	117°	
W8			101°	
at **W8**	W7	W9	NH (β'-521^{Leu}) donor	CO (94^{Ala}) acceptor
distance	2.73	3.09	3.42	2.75
W7		156°	76°	115°
W9			103°	88°
NH (β'-521^{Leu})				106°

Note that 95^{Gly} is an important residue, because the CO as acceptor links the separated W3 and W6 sections of the water chain. Howard *et al*,[26] in examining amino acid sequence alignments from multiple

nitrogenase proteins, have recorded α-95 occurring as many variants, but these side-chain variations should not interfere with the main-chain CO as double hydrogen bond acceptor.

As a prelude to modelling these variable hydrogen atom positions and their movements, it is appropriate to review and understand general Grotthuss mechanisms for proton translocation along a water chain.

3. General characteristics of proton translocation (Grotthuss) mechanisms

The standard concept of the Grotthuss mechanism[27-32] for proton transfer along a chain of water molecules is shown in Fig 6. There are two states, with the configurations of the OH moieties that comprise the chain pointing either forward in the direction of proton transfer (here termed the anterior array), or in the opposite direction (the posterior array). The anterior array can absorb a proton at the entry and release a proton at the exit simply by sliding H atoms along the chain of O-H--O hydrogen bonds. This converts the anterior array to a posterior array. A posterior array is converted back to an anterior array through rotation of each water molecule around the H-O bond that is not in the chain. This rotation, through an approximately tetrahedral angle, passes through a non-hydrogen bonded transition state: in contrast, H atom sliding transitions through a doubly-hydrogen bonded state. The terms 'hop' and 'turn' are sometimes used instead of 'slide' and 'rotation'.

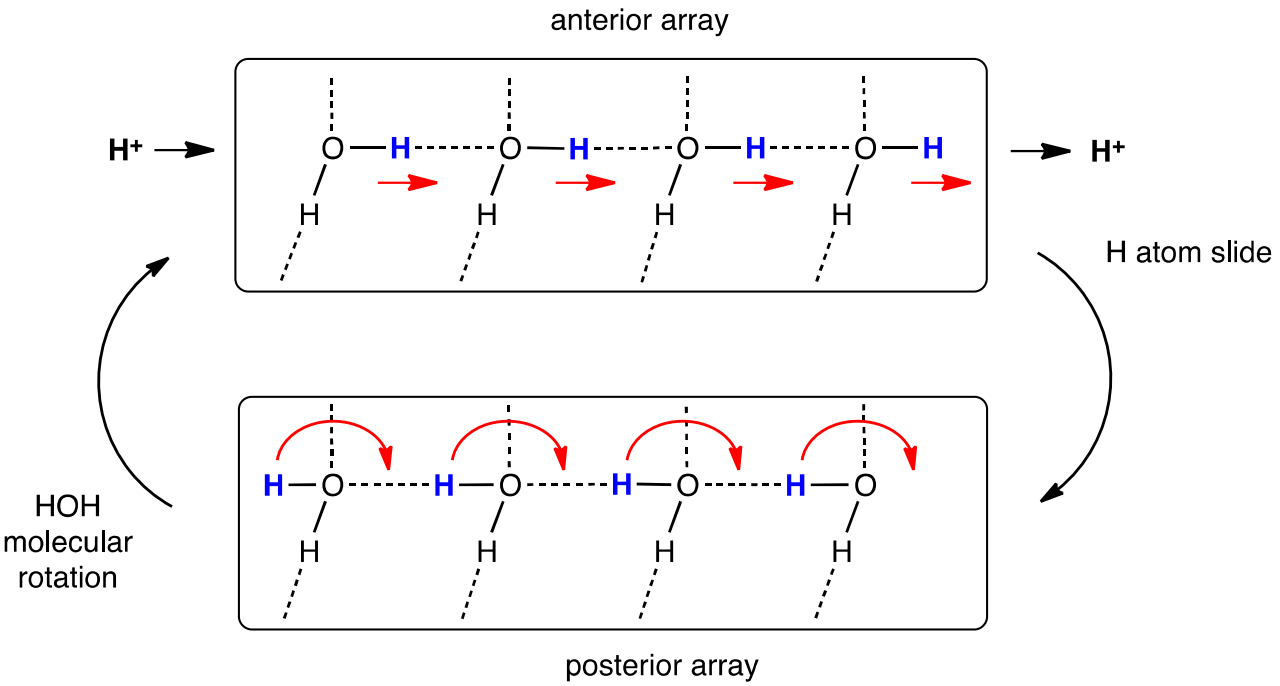

Fig 6. The standard concept for the Grotthuss mechanism, for translocation of a proton from left to right along a chain of water molecules. The H atom slide converts an anterior array of water molecules to posterior, while HOH molecular rotation converts a posterior array to anterior.

The two stages of the process, H atom slide and HOH molecular rotation, are each usually assumed to be concerted, as portrayed in Fig 6, but this is not necessary. A stepwise H atom slide causes a concomitant shift of an H_3O^+ site along the chain. Stepwise HOH molecular rotation generates a pair of non-hydrogen bonded water molecules, as shown in Fig 7.

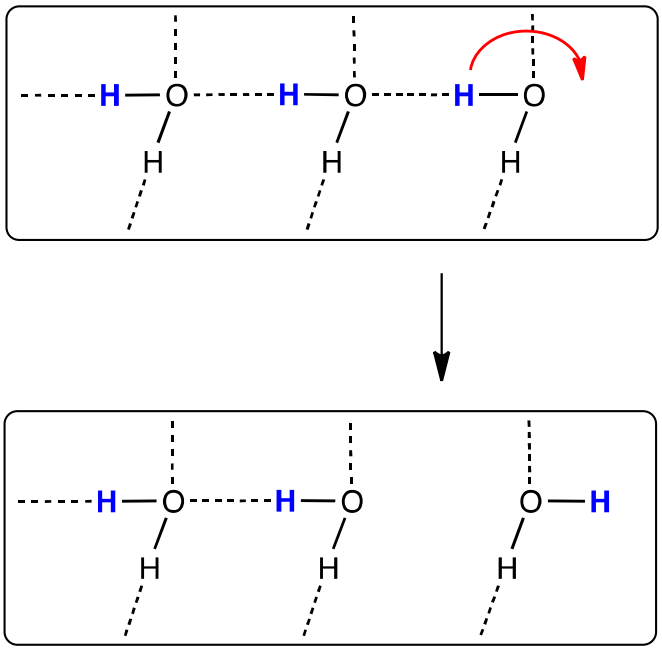

Fig 7. A single HOH molecular rotation generates non-hydrogen bonded contiguous water molecules.

The preceding description assumes that each water molecule in the chain accepts one hydrogen bond from the surroundings and donates one hydrogen bond to the surroundings. Some of these hydrogen bonds can be absent and not affect the H transfer mechanism. However, if a water molecule is involved in two donor or two acceptor hydrogen bonds with the surrounds, the mechanism is disrupted. Fig 8 (a) illustrates a chain water molecule surrounded by two acceptors at the correct tetrahedral positions around a water molecule, such that its H atoms, captured by the environment, are unable to slide or rotate. Fig 8 (b) illustrates a chain water molecule surrounded by two correctly positioned hydrogen bond donors, forcing both its H atoms to be in the water chain, and again preventing the required slide and rotation steps. Here the plasticity of the surrounding medium is relevant: the environment of the chain can be rigid (as in carbon nanotubes[33] or ice), fluid (as in liquid water[28]), or have some plasticity and in proteins and biological membranes.[34,28,35] The plasticity of protein surrounds is understood to allow considerable movement, but not to the extent of changing the specific identities of the surrounding residues. In the present context – protein, plus carboxylate functions of homocitrate, and S in FeMo-co – there are possible variations in the extra-chain hydrogen bonding, as will be described.

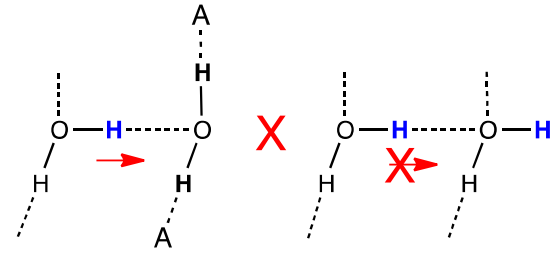

(a)

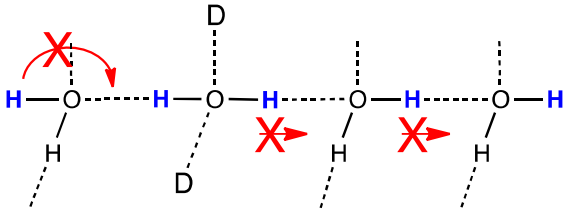

(b)

Fig 8. (a) H atom slide is prevented if one water molecule has both H atoms directed extra-chain. (b) A water molecule with both H atoms directed intra-chain interferes with the slide and rotation operations.

4. Overview: The stages of proton translocation in nitrogenase, and the simulation models

The mechanism for transfer of protons through the water chain towards FeMo-co, followed by the formation of H atoms on FeMo-co and their migration away from the supply site, has three mechanistically different stages. Stage 1 is proton transfer through the chain to atoms, O5 or W1, which are contiguous with S3B of FeMo-co. Stage 2 is the proton transfer to FeMo-co, presumably concomitant with electronation of FeMo-co, forming an H atom on S3B. Stage 3 is reconfiguration of S3B-H in order that the H atom can migrate to other atoms of FeMo-co, and thereby re-prime S3B for acceptance of a subsequent proton and repetition of the cycle. For the proton transfer stages 1 and 2 a computational model (A) containing all of the involved surrounds was used, while for stage 3 the more distant sections of the water chain are not involved or required, and a reduced model (B) was used. These models are displayed in Fig 9, where the marked locations of the H atoms and hydrogen bonds at the water molecules and hca are not significant, being just one of the possibilities explored.

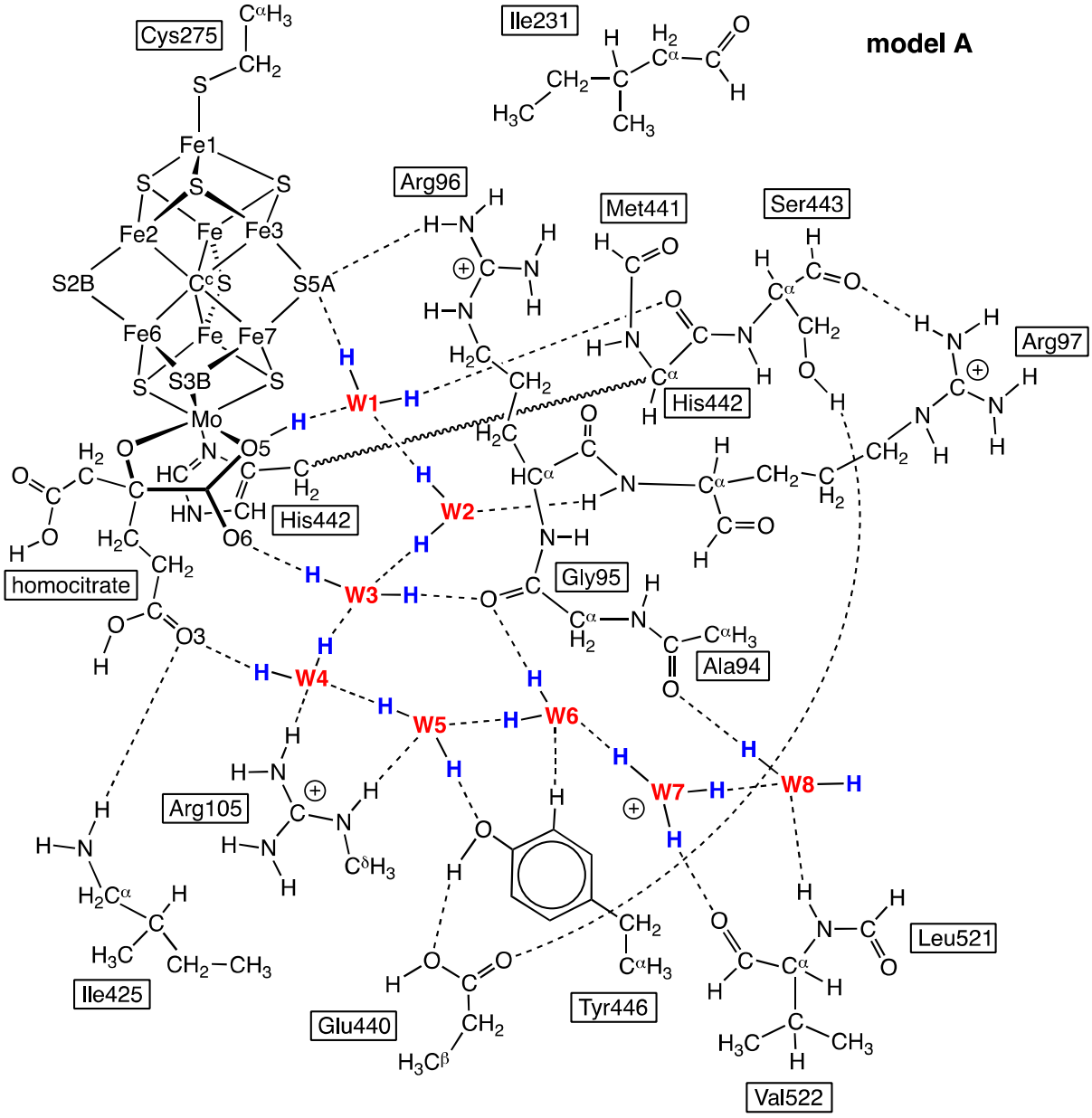
model A
Cys275
Ile231
Arg96
Met441
Ser443
Arg97
His442
homocitrate
Gly95
Ala94
Arg105
Ile425
Glu440
Tyr446
Leu521
Val522
W1
W2
W3
W4
W5
W6
W7
W8
Fe1
Fe2
Fe3
Fe6
Fe7
Mo
S2B
S3B
S5A
O3
O5
O6

(a)

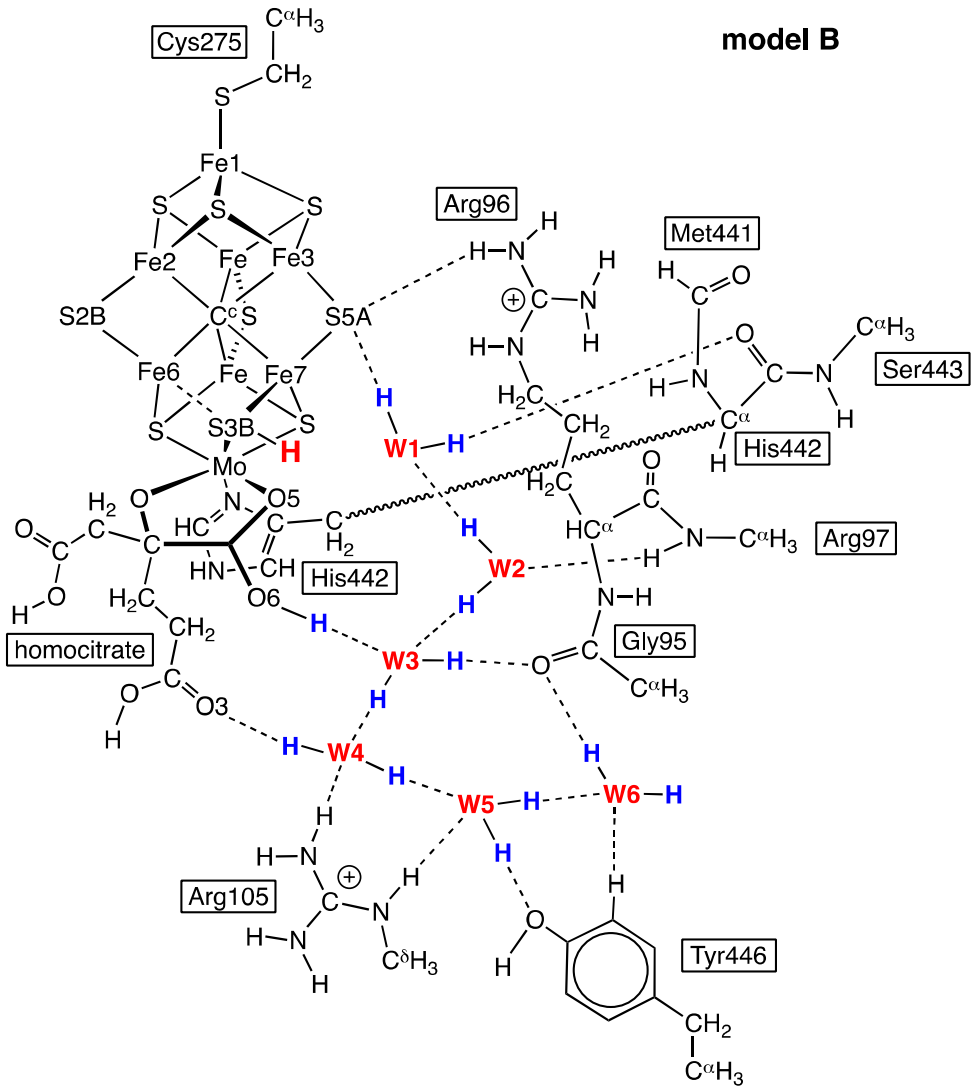

(b)

Fig 9. Schematic representations of the atoms contained in computational models A and B. The Cα-Cβ bond of 442^{His} is elongated (wavy line) in order to clarify the drawings. Dotted lines are hydrogen bonds. Model B is used to assess the configurational changes for the H atom (red) on S3B.

Model A contains 269 atoms and net charge of +1 (for the resting redox state of the FeMo-co core $[Fe_7MoCS_9]^{-1}$[36,37]). Surrounding residues are truncated (with hydrogenation) according to their proximity to the water chain and its hydrogen bonds. Proximal parts of residues 231^{Ile} and 425^{Ile} are included because they provide van der Waals walls for the motions of W1, W2, W4 and W5. Model B omits these barriers, and contains only the essence of the water chain to W6, because the status of the water chain is constant during reconfiguration of S3B-H. Model B contains 162 atoms, with net charge -1.

5. Computational Methods

Density functional (DF) calculations use the DMol methodology of Delley,[38-42] with accurate double numerical (dnp) basis sets.[41] The calculations were all electron, spin-unrestricted, with no imposed symmetry, and employed the BLYP[43,44] functional. The real-space cutoff for calculation of atomic basis sets was 4.76Å, and a fine integration mesh was used. The electronic state of FeMo-co was controlled through the input specification of the signs and magnitudes of the Fe spin densities to be used at the start

of the SCF convergence calculation, and refined in the subsequent optimisation. The stable electronic state adopted for FeMo-co is defined by the spin sign set +, -, +, -, +, +, - for Fe1 through Fe7 (see Fig 1). The net spin S was controlled through occupations of the unrestricted α and β orbitals in the usual way. The COSMO continuum solvation model[45-47] was applied: dielectric constants in the range 5 - 30 had negligible effect on optimised geometries. Incorporation of continuum solvation improved the DF scf convergence in calculations of the large models used here. In the reported results all compared energies were calculated with the same dielectric constant.

Validations Details of the validation of this DMol/BLYP methodology against experimental data have been published for metal sulfide clusters,[48,49] FeMo-co,[50,51,37] and systems with H, H_2 and/or N_2 bound to Fe.[52-54] The calculated internal energy change for $N_2 + 3H_2 \rightarrow 2NH_3$ is -14.8 kcal mol^{-1};[53] Siegbahn[55] states without reference that the experimental value is -17.8 kcal mol^{-1}. The calculated ΔH_f of NH_3 is -12.6 kcal mol^{-1}; experimental -11.9 kcal mol^{-1}.[56] Since the present paper is primarily concerned with hydrogen bonds involving water molecules and carboxylate groups, and the making and breaking of those hydrogen bonds, additional tests of the accuracy of the computational procedures have been undertaken for the benchmark water dimer, the hexagonal water hexamer, hydrated hydronium ion $H_9O_4^+$ and hydrated Zundel ion $H_{13}O_6^+$, and the symmetric acetic acid dimer. The outcomes, detailed with references in the Supplementary Information, are summarised as: (a) O--O distances are accurately reproduced (within 0.02Å) for gas phase systems; (b) the electronic energy for formation of $(H_2O)_2$ calculates as -4.91 kcal mol^{-1}, vs experimentally derived -5.44 kcal mol^{-1}, and is within the range (-4.5 to -5.4 kcal mol^{-1}) spanned by other high-level calculations; (c) the standard gas phase enthalpy of formation of the water dimer is calculated to be -3.19 (298K), slightly less than the experimental measurement (373K) of -3.59 ± 0.5 kcal mol^{-1}; (d) the electronic binding energy of hexagonal $(H_2O)_6$ is in the centre of the range of other high-level calculated values; (e) the O--O separation of the short central symmetrical O-H-O bond of the hydrated Zundel ion is calculated (2.44Å) just shorter than the reported MP2 value (2.49Å); (f) the calculated standard gas phase enthalpy of formation of the symmetrical acetic acid dimer is slightly smaller than the experimental value (-13.4 vs -15.0 kcal mol^{-1}; (g) the calculated gas phase O--O distance in the symmetrical acetic acid dimer (2.69Å) is indistinguishable from the experimental value (2.68Å).

Mapping the potential energy surface The reaction sequences explored here involve the making and breaking of O-H and S-H bonds, and of O-H--O and S-H--O hydrogen bonds. These processes occur within a plastic network of water molecules and protein, and, further, concerted motions of a number of water molecules and their surrounds could be expected. In this context where reaction trajectories and energy barriers can involve multiple geometrical variables, conventional methods for computing transition states along simple reaction coordinates are inappropriate and fragile. Therefore the general approach taken here involves first identification of energy minima, followed by a broad mapping of the potential energy surface between minima, progressing to the relevant saddle-points. This is done using the following pragmatic procedure.[57,58] First a chemically reasonable geometry between energy minima is evaluated by observing the directions and extent of geometry change during an energy minimisation that is restricted to small (ca 0.05Å) atom displacements at each cycle. This reveals both the significant geometrical variables (ie which atoms are moving) and energy gradients, and the direction of the barrier relative the 'reactant' and 'product' minima. Then an atomic arrangement on the other side of this barrier is found (by trial and error and chemical experience) and calculated similarly, revealing any additional moving atoms or variations in hydrogen bonding that are involved in the process and therefore need to be considered in subsequent trials. This provides a rough location of the transition saddle. The third energy minimisation starts from an atom arrangement just back across the trial barrier towards the 'reactant' state. Repetition of this cycle, with subsequent short small-step energy minimisations, *always starting from a point just on the other side of the barrier*, allows the barrier to be straddled from opposing trial positions

that progressively approach each other in geometry and energy, and eventually converge at the transition state (TS). During this iterative procedure the energy gradients diminish, and approach zero at the TS An *essential* component of this procedure is the alternation of trial positions across the barrier, because this automatically leads to optimisation of *all* geometrical variables (including those that are not obvious or are unrecognised during the trial energy-minimisations), and the resulting convergence point is the correct TS, the lowest point on the energy saddle between reactant and product. Confirmation is obtained by following the complete trajectory of geometries from positions nudged just away from the TS, linking the TS with the connected reactant and product energy minima. In practice the procedure is stopped when the energy, geometry and gradient differences between sequential straddling trials become so small as to be chemically insignificant. This pragmatic procedure is laborious, but insightful, and with experience can be made to work efficiently.

Results

6. Optimised model A: protein restraints

In order to retain realistic surrounds for the water chain, model A was first optimised with the positions of some protein atoms fixed: these fixed atoms were Cα of 94^{Ala}, 96^{Arg}, 231^{Ile}, 425^{Ile}, 442^{His}, 443^{Ser}, 446^{Tyr}, β'-522^{Val}, Cβ of 440^{Glu}, and Cδ of β-105^{Arg}. All other atoms, and the position of FeMo-co, were unrestrained. After optimisation there were increases of ca 0.4Å in the distances between these fixed atoms and the central C^c atom of FeMo-co, relative to the crystal structure. The hydrogen bonding distances within the water chain and to its surroundings in the calculated model were close to the crystal distances. This protocol was tested by subsequent release of the constraints. Results are detailed in Table S4, which compares crystal distances with (a) distances in the optimised model with constraints, (b) distances after removal of constraints. Overall the geometrical variations are consistent with normal dynamical variability of proteins.[59]

7. Hydrogen bonding possibilities for W1, W2 and W3

The three water molecules at the FeMo-co end of the chain, W1, W2 and W3, can each have various orientations of their H atoms, and can participate in various hydrogen bonding arrangements. It is necessary to appreciate these variabilities before postulating and testing mechanism for H transfer. Fig 10 pictures eleven structures that illustrate some of the arrangements of H atoms and hydrogen bonds at W1, W2 and W3: all are energy-minimised structures except example 1 which optimises to example 4. In these structures, the pentagonal array O5-W1-W2-W3-O6 containing four hydrogen bonds is a recurring motif. Referring to Fig 10, a number of properties are evident. (a) A donor hydrogen bond from NH of 97^{Arg} to W2 is always present. (b) W1, when involved in a hydrogen bond with W2, can direct H atoms between S3B and O5 (example 1), to O5 and S5A (ex 2), backwards to S4B only (ex 3), to O5 only (examples 4, 5, 6, 7, 9, 10), or to S5A only (eg 8). (c) The CO function of 442^{His} can function as hydrogen bond acceptor from W1, or from W2, or not be involved in hydrogen bonding. (d) W1 and W3 can exist as H_3O^+; a stable intermediate with H_3O^+ at the W2 position has not been found. (e) The weakly basic coordinated carboxylate O5, and slightly more basic O6, can be protonated by H_3O^+ at W1 or W3 respectively, depending on the other hydrogen bonding at W1 and W3. H atom sliding between O5 and W1, and between O6 and W3, is generally a very low energy barrier process: example 5 contains a very short (2.44Å) tight O-H-O bond between W1 and O5. (f) Hydrogen bonding can be absent between W1 and O5 (ex 3, 8, 11). (g) Hydrogen bonding can be absent between W1 and W2 (ex 9) and between W2 and W3 (ex 10). (h) W2 can direct its H atoms towards both W1 and W3 (ex 6, 8): a consequence of this is the blocking of H atom transfer steps through W2 (see Fig 8 (b)).

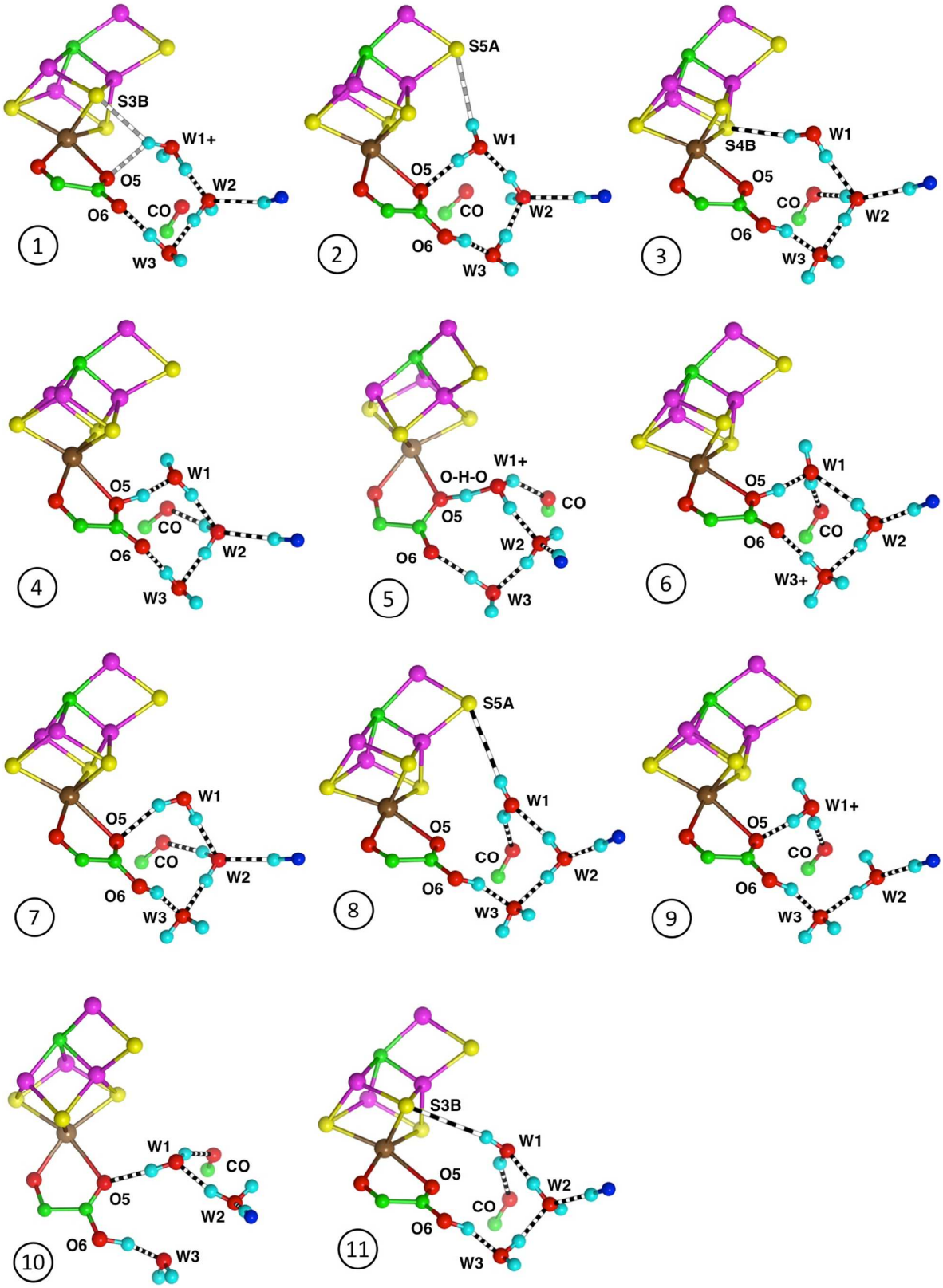

Fig 10. Different arrangements for the hydrogen atoms (cyan) associated with W1, W2 and W3. The various hydrogen bonds with some of (i) O5, O6 of hca, (ii) S atoms S3B, S4B or S5A of FeMo-co, (iii) the carbonyl O of 442^{His} (labelled as CO), are drawn as black/white broken

bonds. In all cases there is a hydrogen bond from NH of 97^{Arg} (marked as dark blue). Parts of FeMo-co, and other atoms of model A, are not shown.

It is clear that W1 is a versatile agent for the transfer of protons to atoms of FeMo-co. This arises because W1 is not required to form a constraining hydrogen bond with any of its neighbours. The geometry of the space containing W1 is propitious for H transfer steps.

The key link to the remainder of the water chain is W3, which is surrounded by four hydrogen bonding entities in tetrahedral array. There are 13 possible configurations for H atoms and hydrogen bonds at W3, shown in Scheme 1 where they are classified according to the anterior/posterior directions of H atoms at W3, W2 and W4. Not all of these are energy minima, but a number of them are part of the mechanisms developed further below. In particular, the isomers with H_3O^+ at W3 generally transfer a proton to O6 if O6 is not already protonated. The carbonyl O of 95^{Gly} accepts a hydrogen bond from W3 in all isomers investigated.

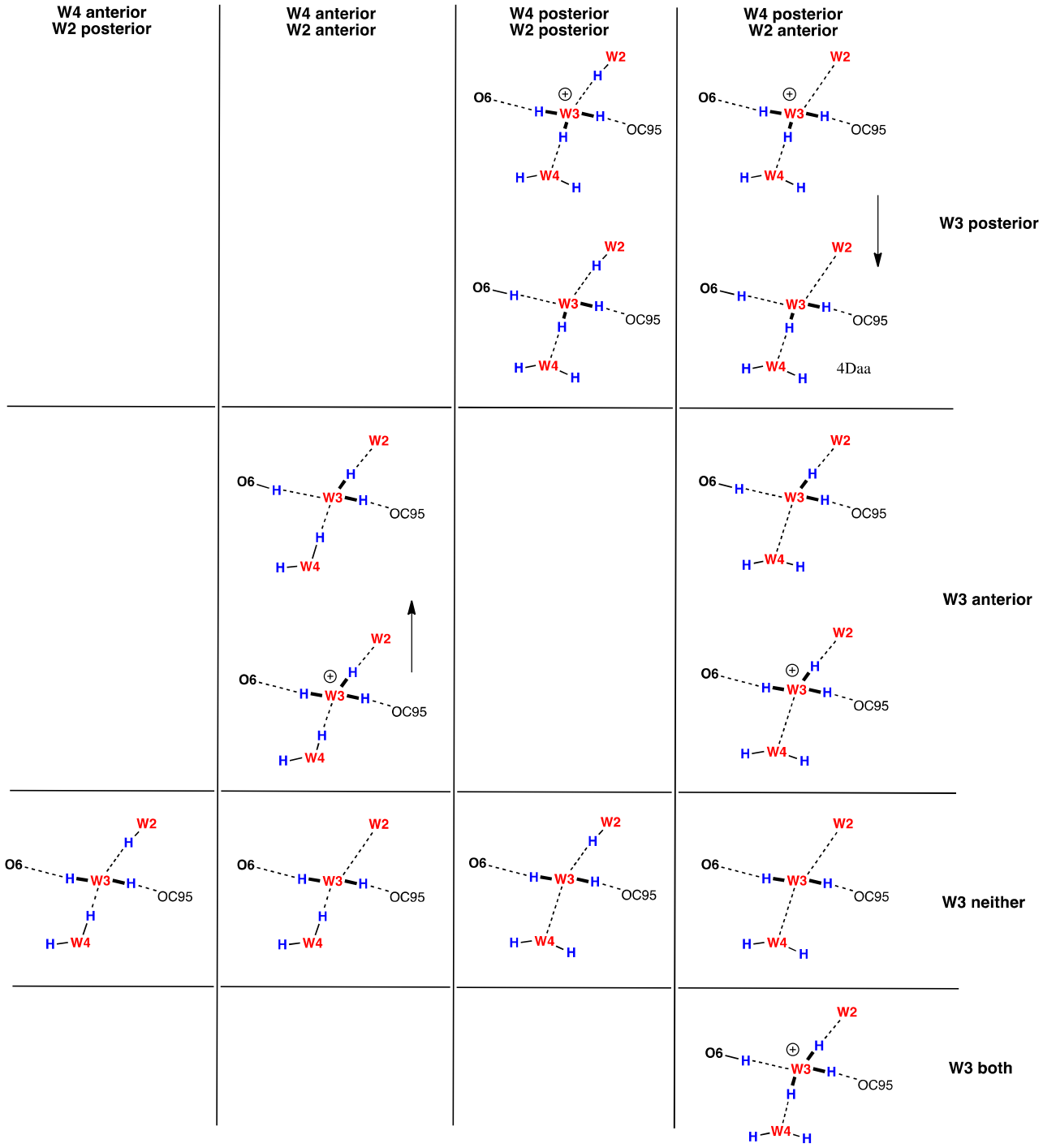

Scheme 1. Possibilities for the locations of hydrogen atoms associated with W3, classified according anterior/posterior directions. Arrows indicate barrierless changes.

8. Hydrogen bonding at W4, W5, W6, W7

At W4 and W5, the hydrogen bonds with surrounds external to the water chain are as shown in Fig 9, for all mechanistic intermediates. W4 donates to O3 of hca and receives from NH_2 of β-105^{Arg}, while W4 donates to OH of 446^{Tyr} and receives from Nε of β-105^{Arg}. At W6 there is one well-defined donation to CO of 95^{Gly}: note that this carbonyl also accepts from W3, and appears to be a significant stabilising connector for the water chain loop W3-W4-W5-W6. The Cε1-H group of 446^{Tyr} points towards W6, at a distance that might be construed as a long, weak C-H--O hydrogen bond, but the angles between this vector and the other hydrogen bonds to W6 deviate strongly from tetrahedral (see Table S5), and the Cε1-

H--W6 interaction is not significant. As shown below, the Cε1-H--W6 vector does not impede rotation of an H atom of W6.

Before exploring extended proton transfer mechanisms, I report some general characteristics of the water rotation steps and proton slide steps that comprise the Grotthuss mechanism in nitrogenase.

9. General characteristics of HOH rotation steps

In order to demonstrate the general principles for rotation steps, a sequence of optimised intermediates connected by rotations of water molecules W3, W4, W5 and W6 is shown in Fig 11. First W3 rotates (around its W3-H--OC95^{Gly} axis) such that the other H changes hydrogen bonding direction from W4 to O6 (intermediate **R1** to intermediate **R2**). Then W4 rotates (about its W4-H--O3 axis) from W5 to W3 (**R2** to **R3**), and similar rotations follow at W5 (**R3** to **R4**) and W6 (**R4** to **R6**). The structure **R5** is the saddle-point for rotation of W6 as it changes from its hydrogen bond to W7 to W5. The HOH geometry does not change during rotation. In each rotation step one hydrogen bond is broken and another is formed, and in the transition domain neither hydrogen bond exists. This is reflected in the optimised geometries (Fig 11 and Table 2). The non-hydrogen bonded distances between water molecules are much larger than 3Å, up to 3.8Å, while the hydrogen bonded distances are ca 2.8Å, the norm.[60] At the transition states, where there are no hydrogen bonds to either contiguous water molecule (or hca O), both adjacent distances are elongated, 3.1 – 3.6Å. Thus, in a sequence of rotation steps along a water-chain there is a ripple of elongating and re-shortening O--O distances.

Table 2 contains the relative energies for the stationary points traversed through this sequence of rotations, showing that the magnitude of the undulations on the potential energy surface is just a few kcal mol^{-1}. The **R5** barrier involves W6 rotating past, but not near, the weak interaction with HCε1(446^{Tyr}) (see Fig 4, Fig 5): the closest H--H approach between W6 and HCε1(446^{Tyr}) is 2.6Å. The angle through which W6 rotates is about 140°, and the energy barrier (5 – 6 kcal mol^{-1}) is larger than the other barriers. The energy variations of Table 2 reflect the energies of the water–water hydrogen bonds involved,[61-63] and their rupture. The flatness of the potential energy surface means that accurate transition states are more difficult to calculate, but are not needed to understand water molecule rotation behaviour. Clearly there is no energy advantage for concerted rotations along a water chain. The full mechanism described below contains details of another sequence of rotations, starting at W3 and ending at W8.

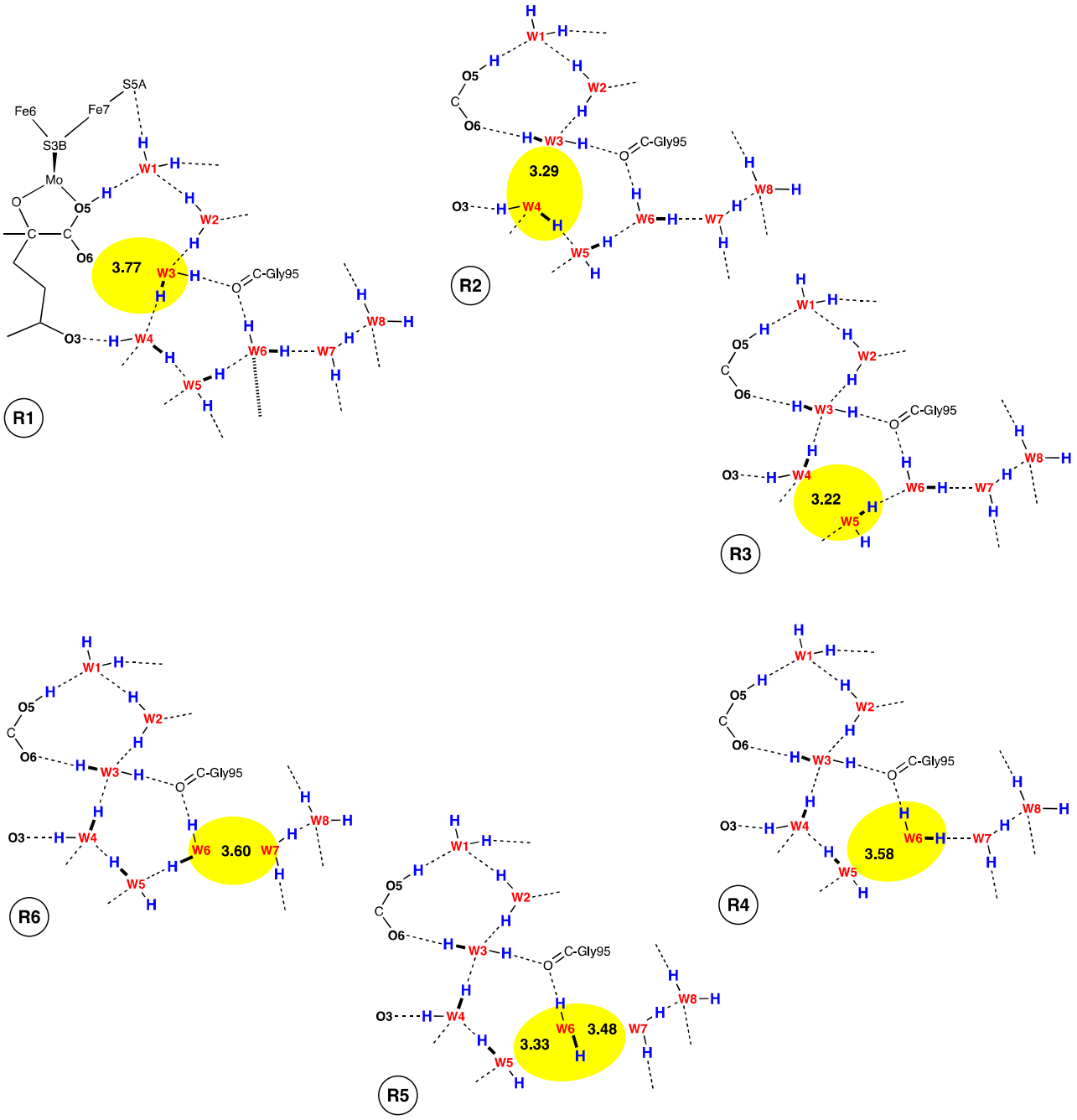

Fig 11. Intermediates in a sequence of rotations of water molecules W3, W4, W5 and W6: **R5** is the transition state between **R4** and **R6**. The elongated O--O distances (Å) are marked.

Table 2. Distances (Å) and relative energies (kcal mol^{-1}) for intermediates and transition states in the sequential rotation of water molecules W3, W4, W5 and W6 shown in Fig 11. Elongated distances are **bold**.

intermediate, transition state	O6--W3	W3--W4	W4--W5	W5--W6	W6--W7	W7--W8	relative energy
R1	**3.77**	2.83	2.79	2.74	2.81	2.87	0
W3 rotating	**3.44**	**3.10**	2.83	2.74	2.80	2.86	3.5
R2, W3 rotated	2.88	**3.29**	2.80	2.74	2.79	2.86	2.8
W4 rotating	2.94	**3.11**	**3.43**	2.76	2.79	2.85	5.4
R3, W4 rotated	2.83	2.91	**3.22**	2.75	2.80	2.85	2.2
W5 rotating	2.80	2.81	**2.97**	**3.34**	2.85	2.85	4.5
R4, W5 rotated	2.82	2.81	2.83	**3.58**	2.83	2.85	3.8
R5, W6 rotating	2.81	2.83	2.83	**3.50**	**3.62**	2.88	9.7
R6, W6 rotated	2.82	2.82	2.77	2.91	**3.60**	2.92	4.8

10. General characteristics of proton slide steps

Fig 12 shows a sequence of intermediates involving proton slides, from W7 (**S1**) to W6, W5, W4, W3 and then O6 (**S6**). These slides shift an H_3O^+ site through the water chain, from $W7^+$ through to $W3^+$, and finally $W3^+$ protonates O6 of hca (the symbol Wn^+ is used hereafter to indicate that Wn is H_3O^+). Table 3 reports the distances between water molecules in the chain, and the relative energies of the intermediates. The main result is that H_3O^+ contracts its hydrogen bonds to the two contiguous water molecules, from the normal hydrogen bonding distance of ca 2.8Å, to ca 2.5Å. As each proton slides from its anterior position to posterior position, the water molecules in the water path contract towards the location of H_3O^+, and the contraction relocates along the path. In **S6** the hydrogen bond between O6-H and W3 is not as short (2.6Å) because there is no formal H_3O^+.

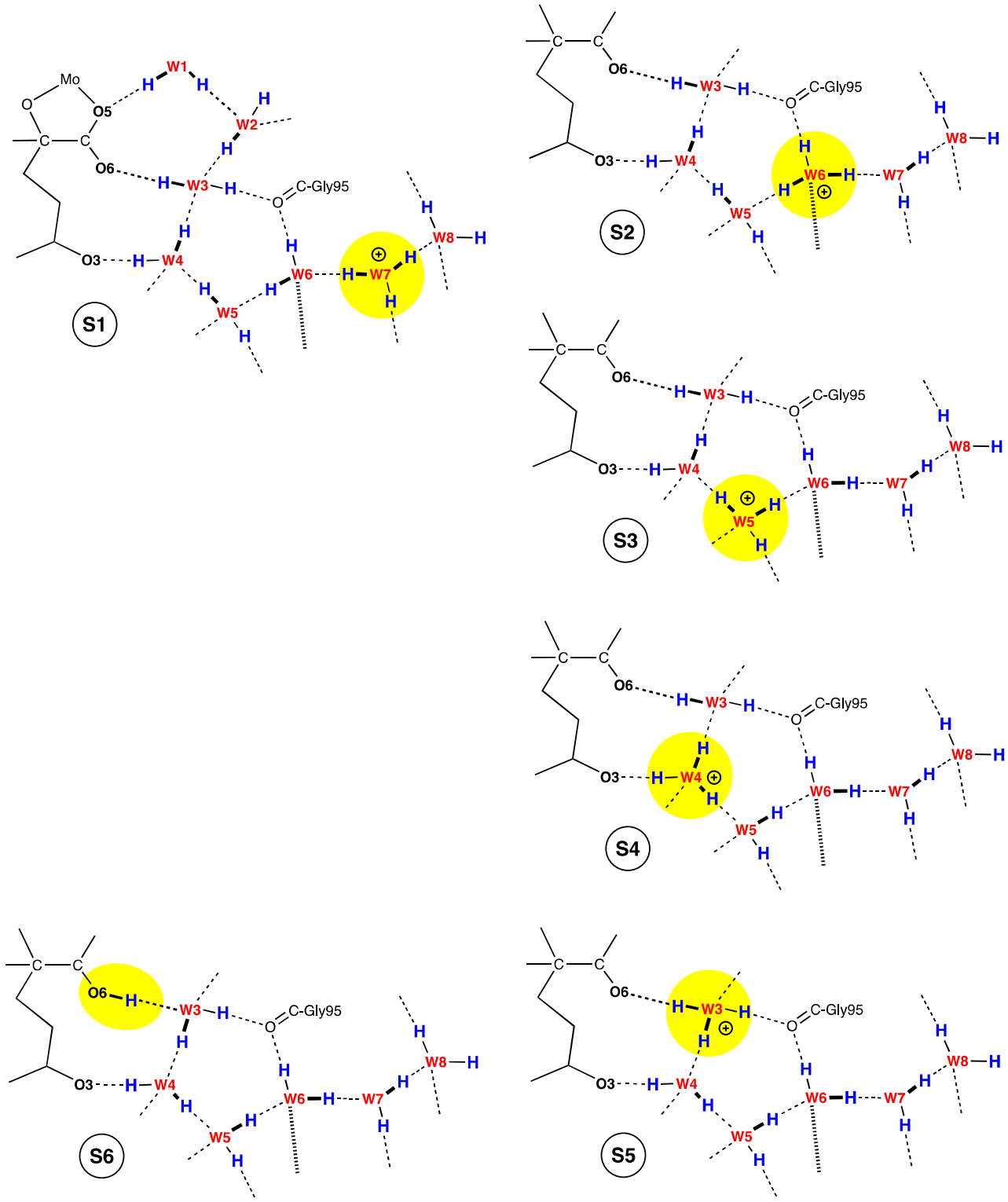

Fig 12. Intermediates in the series of proton slides, from W7 to O6 of hca. The invariant arrangement of other H atoms at W2 and W1 is shown for **S1**.

The more stable locations for H_3O^+ are W6 and W3. The lower stability of H_3O^+ at W5 and W4 is attributed in part to the hydrogen bonding geometry: the hydrogen bonds between W5 and W4 are bent by 20 –30°. In addition, the external hydrogen bonds engaged by W5 and W4, to 446^{Tyr} and hcaO3, are geometrically opposed to the direction of W5-H-W4 hydrogen bonds, and therefore could inhibit W5--W4 shortening.

Table 3. Relevant distances (Å) and energies (kcal mol^{-1}) of optimised intermediates in the series of proton slides, from W7 to O6 of hca (see Fig 12): the symbol Wn$^+$ indicates that Wn is H_3O^+.

intermediate	W8--W7	W7--W6	W6--W5	W5--W4	W4--W3	W3--O6	relative energy
S1 W7$^+$	**2.58**	**2.49**	2.77	2.77	2.81	2.67	0
S2 W6$^+$	2.75	**2.54**	**2.60**	2.72	2.81	2.66	-2.5
S3 W5$^+$	2.77	2.66	**2.52**	**2.56**	2.77	2.69	7.5
S4 W4$^+$	2.80	2.73	2.62	**2.52**	**2.51**	2.62	7.4
S5 W3$^+$	2.82	2.75	2.66	2.60	**2.52**	**2.49**	4.5
S6 O6-H	2.85	2.80	2.72	2.76	2.76	2.60	-5.3

The preceding slide, W7 to W3, was calculated as a sequence of individual proton movements. The potential energy barrier arises in the less stable W5$^+$ and W4$^+$ intermediates. A different slide operation, from O6 to W3 to W2 to W1 to O5, was found to proceed as a concerted atom movement, with one transition state, as shown in Fig 13 converts hca protonated at O6 to hca protonated at O5. The transition state is 7.3 kcal mol^{-1} above the two limiting configurations. The distances marked in Fig 13 show the geometrical asymmetry of the TS, in which the first H is almost completely transferred to W3 and the last H is still to be moved from W1: the movements between W3--W2 and W2--W1 are partial. A feature is the tight hydrogen bonding at the TS, with the W3--W2 separation only 2.46Å, and W2--W1 only 2.48Å. These short distances are the same as those observed experimentally in other systems.[64,65]

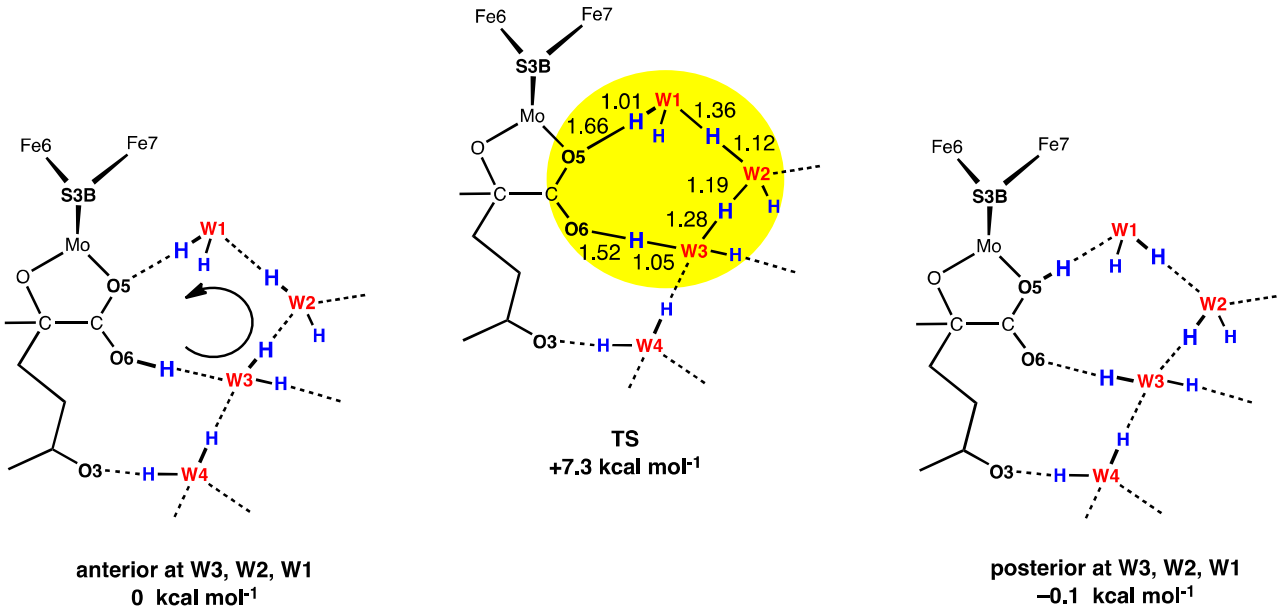

Fig 13. A concerted proton slide with a single transition state: distances (Å) and relative energies (kcal mol^{-1}) are marked.

11. H transfer to S3B

The essential step in the overall process is transfer of a proton to FeMo-co, with S3B the most likely recipient atom. Water W1 and O5 of hca are the two sites close to S3B that are capable of bearing protons, and are potential transfer agents. Scheme 2 (a) outlines possible pathways that could contribute to proton transfer to S3B via W1 or O5. The path from O5 to S3B, while attractive geometrically, has a

disability that makes it very unlikely. The saddle-point for this transfer, which can also incorporate an interaction with W1 as shown in Scheme 2 (b), is connected on the potential energy surface to an O5-H structure that has irregular geometry at O5. The pathway down the potential energy surface from the saddle-point continues past this irregular structure by full dissociation of the O5-H moiety from Mo. The essential difficulty here is that the bonding stereochemistry at O5 that is needed to pass H to S3B is incompatible with the stereochemistry of O5 bonded to Mo. Alternatively stated, Mo and the proton transferring to S3B compete for the same lone pair orbital on O5. The Mo coordination of O5 required for its position close to S3B is incompatible with the required C-O-H geometry at O5. Therefore, because a suitable precursor intermediate is not available, this proton transfer pathway from O5 to S3B is discounted.

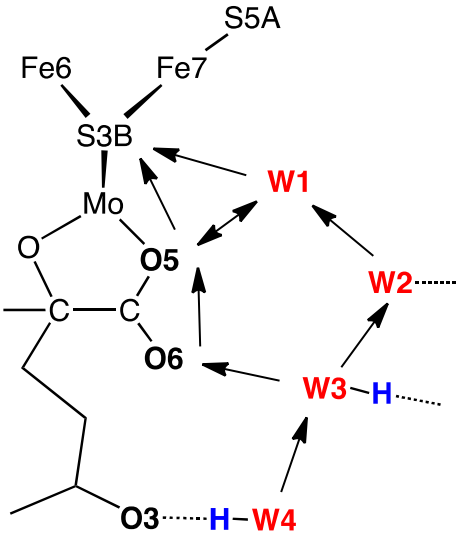

(a)

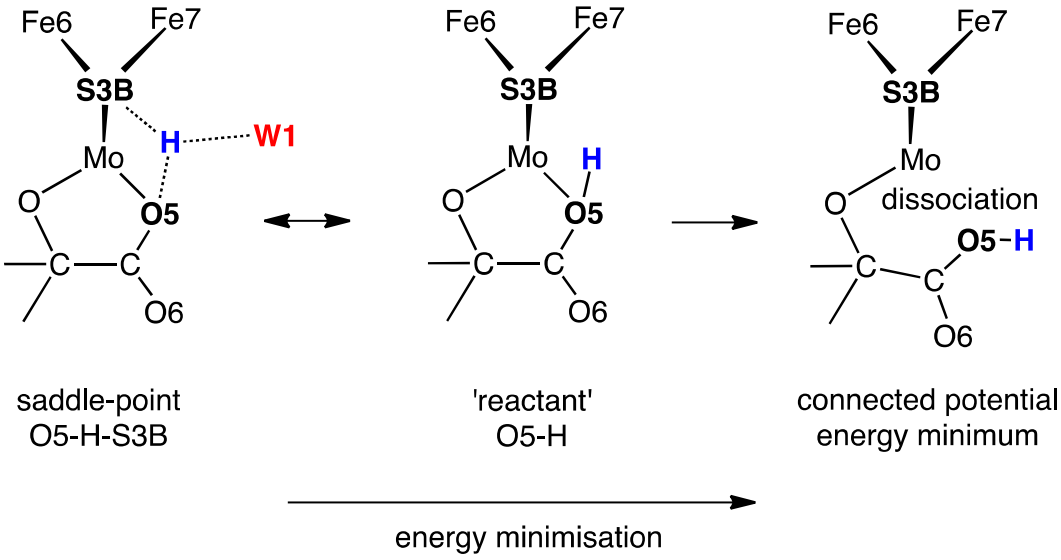

(b)

Scheme 2. (a) Possible pathways for H transfer to S3B. (b) Direct transfer from O5 to S3B is thwarted by connection to an inappropriate energy well with O5-H dissociated from Mo.

Proton transfer from W1 directly to S3B is stereochemically favoured, at both W1 and S3B, provided that the water molecule at W1 does not direct one O-H towards S5A (the S5A-W1-S3B angle is too small, *ca*

60°). Also, the W1 to S3B transfer requires that O5 not be protonated (for geometrical reasons). W1 must be in a protonated state, H_3O^+, to be able to transfer a proton to S3B.

The favourable trajectory from W1 to S3B passes through the transition state shown in Fig 14, and Table 4 provides key metrics. The atoms that move in passage through the TS are Fe6--S3B--H--W1, in approximately linear sequence. At the TS, H^a on W1 (see Fig 14) is not directly hydrogen bonded to any other atom (and neither is H^b at W2). This transition state has been determined for two redox states of FeMo-co (the standard resting state, S=3/2, and the one-electron reduced state, S=1). The overall electron population affects the character of the TS, in that reduction by one electron has the H atom shifted towards W1 in the TS (Table 4). That is, S3B is able to capture the proton from H_3O^+ at a longer distance when the complete system is reduced by one electron. This is because electronation increases the negative charge specifically on S atoms of FeMo-co:[66,67,53] charges on other atoms in the system are unaffected by electronation (Table 4).

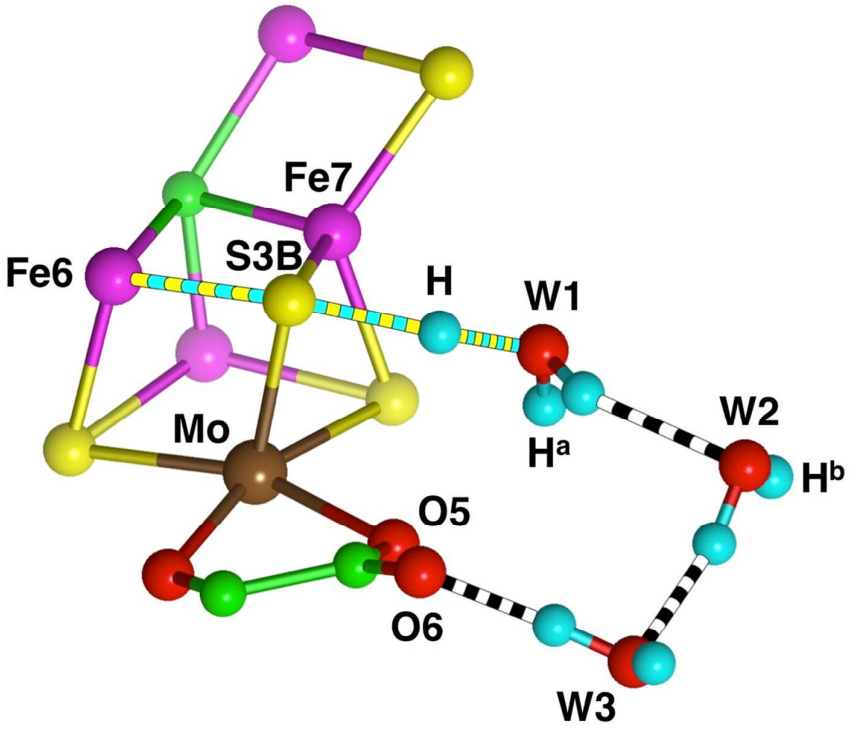

Fig 14. Transition state for transfer of H from $W1^+$ to S3B. The changing bonds are marked yellow/cyan; black/white are hydrogen bonds.

Table 4. Distances (Å) and Mulliken atomic charges at the transition state for H transfer from $W1^+$ to S3B.

TS	resting state	one-electron reduced
	S=3/2	S=1
	distances	
H - S3B	1.69	1.78
H - W1	1.30	1.22
S3B - W1	2.98	2.99
S3B - Fe6	2.58	2.58
W1 - O5	2.82	2.82
W1 - W2	2.99	3.06
	charges (Mulliken)	
S3B	-0.74	-0.80
H	0.38	0.38
O of W1	-0.47	-0.43
Fe6	0.58	0.57
O5	-0.62	-0.62
Fe7	0.58	0.57
Mo	0.92	0.90
S4B	-0.65	-0.72

Characteristics of the trajectory for H transfer from $W1^+$ to S3B are shown in Fig 15. The W1--S3B distance, 4.05Å in resting protein, shortens to ca 3Å during the transfer, and this property is analogous to the shortening that occurs during proton slides between water molecules. As the S3B-H bond is formed the S3B-Fe6 bond lengthens, as is characteristic of the protonation of bridging S atoms in metal sulfide clusters.[68,69] Continuation of the transfer trajectory beyond the central stage shown in Fig 15, takes reactant $W1^+$, and product W1, into the spaces in which they are relatively fluid and able to reorient their hydrogen bonds. These further changes are indicated by the continuing energy changes at the limits of Fig 15. In the reactant stage for the transfer, where W1 is H_3O^+, energy minimisation occurs through reorientation of $W1^+$ to form a hydrogen bond with O5, and then transfer of a proton to O5. In the product stage of the transfer, W1 reorients first to form donor hydrogen bonds to S4B and W2, and then reorients further to form donor hydrogen bonds to O5 and W2. These reorientations of $W1^+$ and W1 that precede and follow the essential proton transfer from $W1^+$ to S3B are considered further below as part of the full mechanism.

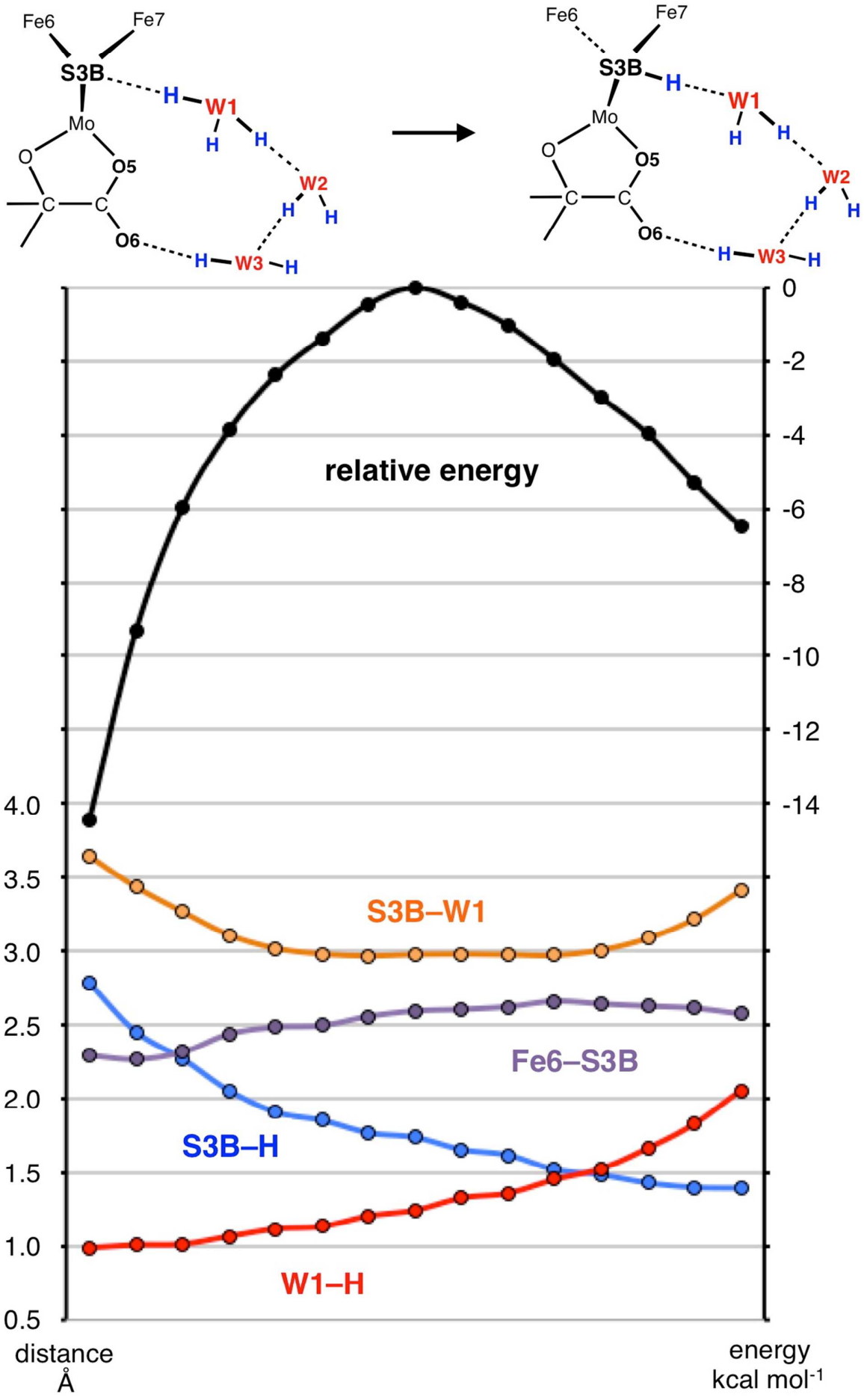
Fe6
Fe7
S3B
H
W1
Mo
O
O5
C
C
W2
O6
W3
relative energy
S3B–W1
Fe6–S3B
S3B–H
W1–H
0
-2
-4
-6
-8
-10
-12
-14
4.0
3.5
3.0
2.5
2.0
1.5
1.0
0.5
distance
Å
energy
kcal mol-1

Fig 15. Points on the central section of the trajectory for proton transfer from W1+ to S3B, as calculated for the resting S=3/2 state of FeMo-co.

12. Reconfiguration of S3B-H, and recovery of S3B

Protonation of triply-bridging S3B elongates the S3B-Fe6 bond and forms doubly-bridging S3B-H in the *exo*-configuration: that is, the S3B-H bond of pyramidal S3B is *exo* to Fe6. The reconfiguration of stereochemistry around S3B is readily achieved by concerted lengthenings and shortenings of the bonds between S3B and its three Fe neighbours. These rearrangements have been described computationally for FeMo-co (with a simplified *in vacuo* model)[70] and in more detail for $Fe_4S_4X_4$ clusters.[69] Here the reconfiguration of S3B-H has been recalculated with a more elaborate model B (see above). The essential results are shown in Fig 16. There are four stable configurations, **3b2**, **3b3**, **3b5** and **3b6**, in each of which S3B-H has pyramidal stereochemistry, and one of the S3B-Fe distances is elongated by 0.4 – 0.6Å. In **3b2** and **3b6** the S3B-H bond is *endo* to the more distant Fe atom, while in **3b3** and **3b5** this relationship is *exo*. These four energy minima are connected by four transition states, in which the S3B-Fe distances equalise before transitioning to elongation of the other S3B-Fe bond. The interchanges of the S3B-H configurations occur *not* by passage through a planar Mo-(S3B-H)-Fe intermediate, but by lower energy processes involving weakening of Fe-SH bonds and small movements of the H atom. Note that the **3b2** ↔ **3b3** and **3b5** ↔ **3b6** barriers are < 3 kcal mol^{-1}. Note also that the transition states for **3b2** ↔ **3b6** and **3b3** ↔ **3b5** involve approximately tetrahedral stereochemistry at S3B, and are 8 – 11 kcal mol^{-1} higher in energy. These characteristics of S3B-H in FeMo-co are the same as those calculated for the protonation of μ_3-S in other metal sulfide clusters. In the present context, the significant result is that S3B-H as formed by H transfer from W1, in the **3b5** configuration, is able to isomerise to a configuration such as **3b3** or **3b2** in which the H atom is on the side of S3B opposite to W1.

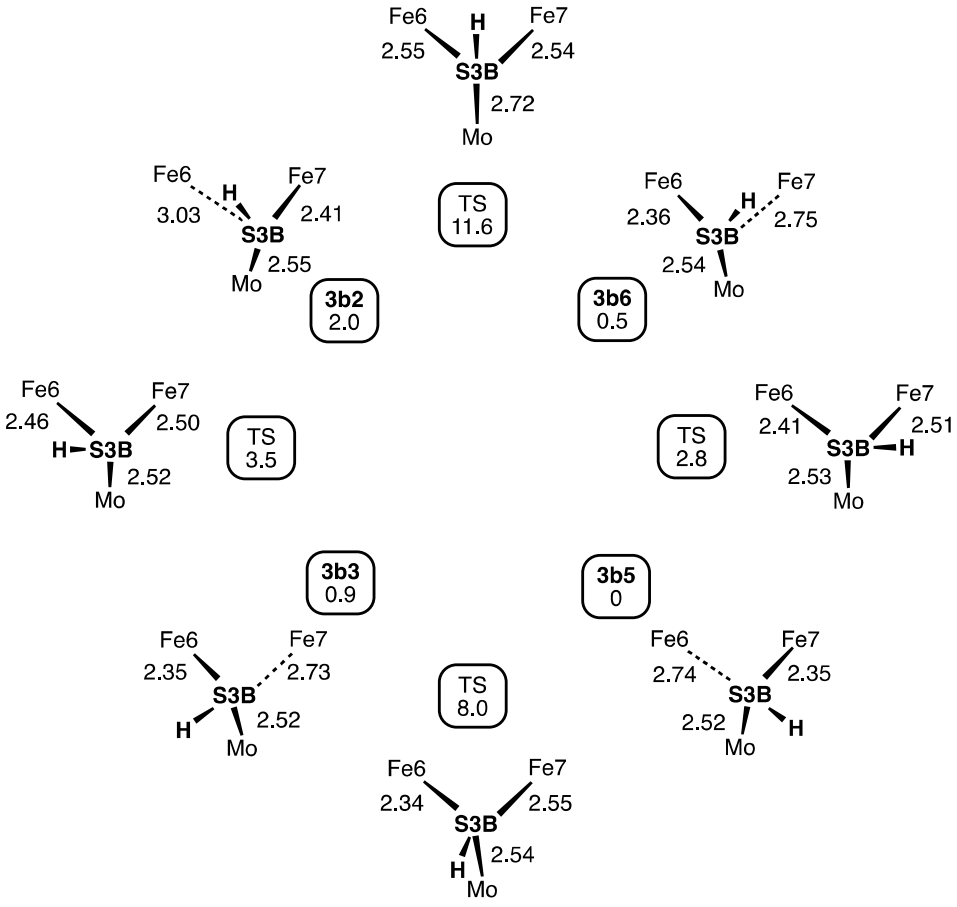

Fig 16. The configurations of S3B-H. Structures **3b2**, **3b3**, **3b5** and **3b6**, with pyramidal Mo-(S3B-H)-Fe stereochemistry, are the energy minima: the other four structures are the transition states that connect them. Fe-S and Mo-S distances (Å) are marked, and the numbers in the boxes are relative energies (kcal mol^{-1}).

The H atom on S3B in configuration **3b2** is readily able to migrate to Fe6, towards which it is directed. Using the same model B, the barrier for this is calculated to be just 4.2 kcal mol^{-1}, and the product with H in the *exo* coordination position of Fe6 is 13 kcal mol^{-1} below the saddle point. This last step returns S3B to its resting triply-bridging state, ready to receive a subsequent H atom from the proton transfer chain.

13. Construction of a complete mechanism

The complete mechanism is envisaged as a cycle with the following components (a) introduction of a proton at the distal end of the proton path (W8), (b) movement of a proton through the water chain to W1, the precursor for transfer to S3B, (c) addition of an electron to FeMo-co, (d) H transfer to S3B, (e) reconfiguration of S3B-H, and migration of H to other atoms of FeMo-co away from S3B, (f) rearrangement of the water chain in order to repeat the cycle. These events need not occur in this temporal sequence. Another factor in the formulation of the full mechanism is the differentiation of sections of the proton path, and recognition that H_3O^+ is stabilised at the W6, W3 and W1 positions of the water chain. Also, O6 and O5 of hca are relatively basic sites that can be protonated by H_3O^+ occurring at positions W3 and W1 respectively: O6 and O5 provide a buffering facility for the proton translocation mechanism.

Consideration of possible sequences of events has generated a general mechanism with the intermediates and steps outlined in Fig 17. In order to clarify the presentation, this mechanistic sequence will be outlined first without elaboration, and then the geometrical and energetic properties of the potential energy surface for the component steps will be developed in more detail.

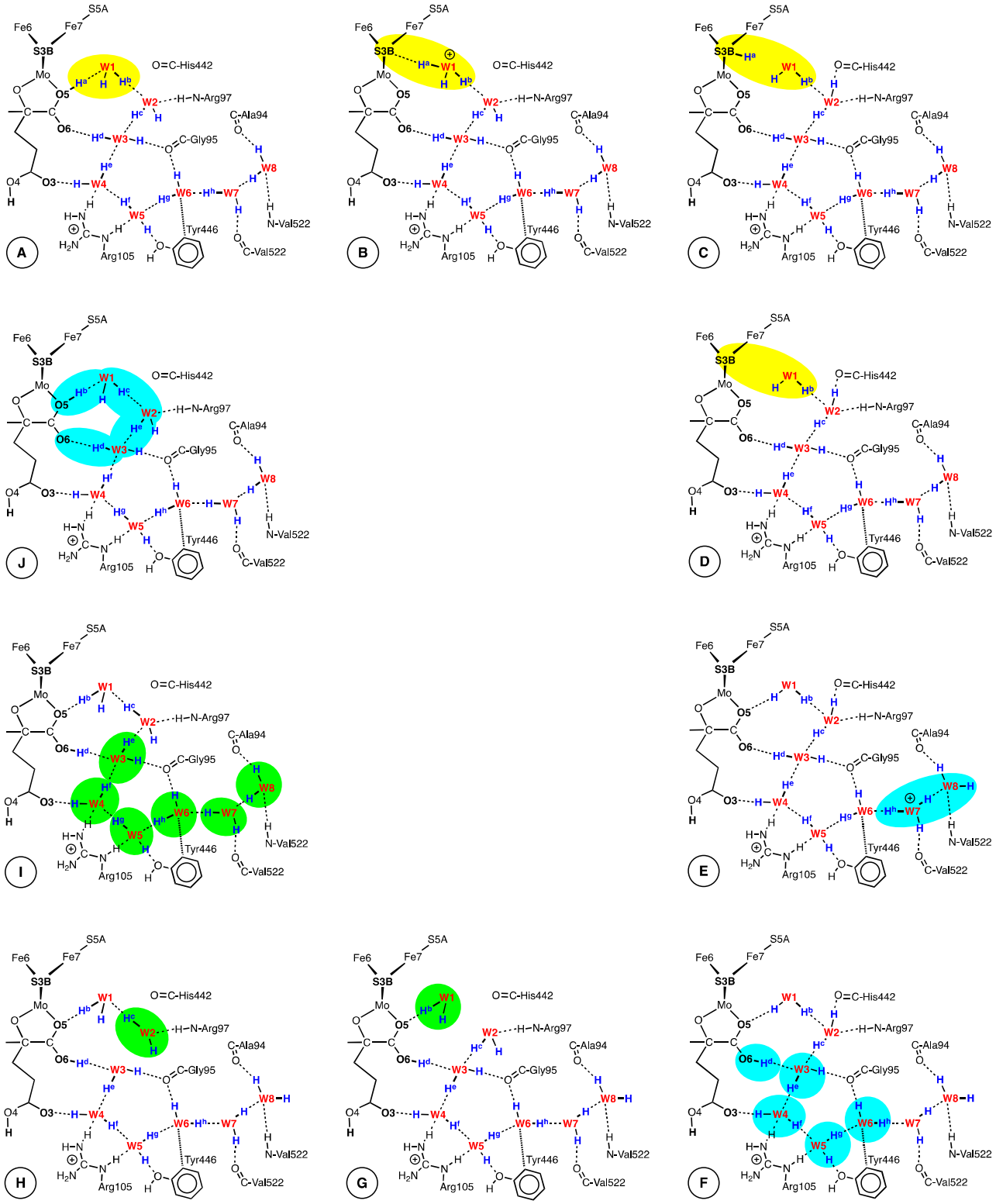

Fig 17. The main intermediates and steps in the proposed mechanism. Yellow background highlights steps that occur at W1 and S3B, including reorientation of W1 and H transfer to S3B; cyan backgrounds highlight H slide steps that have occurred from the previous intermediate; green backgrounds highlight rotations of water molecules that have occurred from the previous intermediate.

State **A** could be regarded as a resting state: the FeMo-co electronic state is S = 3/2. Structure **A** is relatively stable, mainly because O5 has been protonated by H_3O^+ at W1. In order to prepare the geometry for H transfer to S3B, state **B** needs to be reached, by reversing the protonation of O5, and re-orienting H_3O^+ at W1 so that one O-H bond is directed towards S3B. This change involves W1 moving

close to O5, then H slide to W1, and some rotation of W1, and it occurs as a single trajectory, with no intermediate energy wells. State **B** is *ca* 12 kcal mol^{-1} less stable than **A**. About 2 kcal mol^{-1} of this energy difference is associated the H slide to W1, about 5 kcal mol^{-1} is the cost of W1^{+} moving away from O5, and about 5 kcal mol^{-1} is associated with re-orientation of W1^{+}.

State **B** (also S=3/2) is the precursor for H transfer from W1^{+} to S3B, resulting in intermediate **C**. This transfer has been described above (section 11). At some point in the conversion from **B** to **C** it is presumed that an electron is added to FeMo-co, via the P-cluster, using the separate electron transfer machinery. It is presumed also that protein dynamical changes provide the linkage between electron transfer to FeMo-co, and proton transfer to S3B, but the present modelling does not contribute to these questions. As already mentioned (section 11) electronation of FeMo-co concentrates negative charge on its S atoms, favouring proton transfer from W1^{+} to S3B. Intermediate **C** is modelled as containing an H atom on S3B, comprised of the proton transferred from W1^{+} and the added electron. The atom charges for H atoms on FeMo-co have been described in more detail elsewhere.[71] The stable electronic state of **C** is calculated to be S=1.

Intermediate **D** is the result of the subsequent reconfiguration of S3B-H and the migration of the H atom away from S3B, as described in section 12. The computational models of **D** and subsequent intermediates do not include this migrated H atom, because it is not part of the proton transfer through the water chain. The electronic state of **D** is calculated to be S=3/2.

The next step is addition of a proton at the W8 end of the water chain. In **D** the water molecule at W8 has the anterior configuration, and so is ready to receive a proton from the more distant part of the water chain, ie W9 which is not explicitly modelled. This proton addition causes a spontaneous proton slide from W8 to W7, and the stable intermediate at this point is **E**, which contains W7^{+}. The stable electronic state is still S = 3/2, and this electronic state is preserved throughout the remainder of the mechanism.

At this stage the water molecules W7, W6, and W5 are configured anterior, W3 is anterior towards O6 but not W2, and W2 and W1 have the posterior configuration. In order to recover the starting state, that is to transform intermediate **E** with H_3O^{+} at W7 to intermediate **A** with H_3O^{+} at W1, the Grotthuss mechanism requires that there be slides and rotations at all water molecules from W7 to W1. For those water molecules with anterior configuration the slide must precede rotation, and vice versa for those with posterior configuration. Since the proton pressure is from W7^{+}, the slides from W7 through anterior W6, W5, W4 and W3 are introduced next. These are the sequential slides already described above in Fig 12 and Table 3, concluding with protonation of O6 by W3^{+}. The outcome is intermediate **F**, which is 5 kcal mol^{-1} more stable than intermediate **E**.

At intermediate **F** all water molecules are in the posterior configuration, and therefore are primed for rotation steps. It is necessary that rotations occur starting at the front end of a sequence of such posterior water molecules (Fig 7). As already described, water rotations are characterised by flat energy surfaces and increased W--W separations, and so are not tightly concerted. Therefore the first rotation for intermediate **F** occurs at W1, rotating from W2 to O5, leading to intermediate **G**. The saddle point for this step is difficult to pinpoint because the energy surface is so flat, but the barrier is less than 2 kcal mol^{-1}. Then W2 can rotate forward to yield intermediate **H** (Fig 17), and the barrier for this is also less than 2 kcal mol^{-1}. The small energy changes involved in these rotation steps at W1 and W2 are comparable with the general re-orientation energies for the orientationally fluid water molecules W1 and W2. Note that in **G** and **H** both W1 and W2 each have one O-H bond not specifically hydrogen bonded to a surrounding acceptor. There is another energy minimum in this spatial domain, in which W2 directs its O-H bonds anterior to W1 and posterior to W3: this is the configuration illustrated in Fig 8 (b), that blocks proton transfer, and is to be avoided.

Once W2 has rotated forward (**H**) and W2--W3 is 'empty', W3 can rotate from posterior to anterior while maintaining its donor O-H hydrogen bond to OC-95^{Gly} and acceptor hydrogen bond from O6-H. This can then be followed by rotations at W4, W5, W6, W7 and W8, reaching intermediate **I**. This sequence of rotations is similar to that described above in Fig 11 and Table 2, in that an absence of hydrogen bonding between contiguous water molecules moves backward through the water chain, and translations (as well as rotations) of water molecules occur because each non-hydrogen bonded water pair is separated by larger distances up to 3.6Å. Note that the sequence of rotations between intermediates **H** and **I** differs from that in Fig 11 because the O5--W1--W2--W3--O6 cycle is configured differently. The potential energy surface undulates through the **H** $\rightarrow$ **I** sequence as: W3 posterior = 0 kcal mol^{-1}, W3 rotation saddle point = +5.9 kcal mol^{-1}, W3 rotated = +2.7 kcal mol^{-1}, W4 rotated = +0.4 kcal mol^{-1}, W5 rotated = +4.7 kcal mol^{-1}, W6 rotation saddle point = +9.7 kcal mol^{-1}, W6 rotated = +3.9 kcal mol^{-1}, W7 rotated = +3.4 kcal mol^{-1}, W8 rotated -2.0 kcal mol^{-1}. As previously, high accuracy has not been sought because the surface is relatively flat.

The last stage, intermediate **I** to intermediate **J**, involves proton slides from O6 to W3 to W2 to W1 to O5, and these occur in concert as already described in Fig 13.

This completes the cycle: intermediate **J** has the same arrangement of protons as state **A**, and passage to it has moved a proton (with concomitant electron) onto FeMo-co and replenished the proton by addition at W8. The whole cycle is energetically fairly flat, with the largest potential energy barrier occurring in the preparation for transfer of a proton from W1^{+} to S3B. The proton has to be extracted from O5 onto W1 and then directed towards S3B, and the energy barrier here reflects the greater basicity of O5 over S3B. Excluding the effect of electron addition during this process, that is by comparison of models with the same electron population, the energy step from state **A** to the saddle-point for H transfer to S3B is +14 kcal mol^{-1}, and this is the largest barrier in the complete cycle.

Discussion

The water path from the surface of the MoFe protein of nitrogenase to its active site FeMo-co has been modelled in more detail than previously, with explicit inclusion of all relevant surrounding residues. The bond-making and bond-breaking processes that are involved in the translocation of a proton along the strictly conserved inner section of eight water molecules and onto FeMo-co have been characterised through density functional simulations using a model containing 269 atoms. Some of the proton shifts are typical of the slide and rotation phases of a standard Grotthuss mechanism, while other steps are specific to the nitrogenase structure. In particular, the proton buffering actions of O5 and O6 of homocitrate are unique, and O3 of homocitrate is also involved. Another key property of the nitrogenase water chain is the orientational versatility of W1 immediately adjacent to FeMo-co, and the hydrogen bonding versatility of W2 and W3. Electronation of FeMo-co is also a key aspect of nitrogenase reactivity. The modelling supports the hypothesis that addition of an electron to FeMo-co is coupled temporally with its protonation, such that an H atom is added to FeMo-co.

After consideration of alternatives at the various stages of the mechanism, a specific mechanism containing 20 individual steps is proposed. For most of this mechanistic sequence the potential energy surface is remarkably flat, undulating by < 5 kcal mol^{-1}. The largest potential energy barrier is estimated to be 14 kcal mol^{-1}, for the preparation of H_3O^{+} at the W1 position in order to reach the saddle-point for proton transfer to S3B. While state **A** is suggested as the resting state, the protein could rest at other intermediates.

This proton translocation mechanism is capable of the serial hydrogenation of FeMo-co that is required in the full catalytic cycle for the physiological reduction of N_2, and for the majority of other substrates of nitrogenase.[72,15] Indeed, the mechanism proposed here is capable of delivering an unlimited number of

protons to FeMo-co, for the various reactions catalysed there. It has been suggested that the side-chain Nε-H of 195^{His}, which is within hydrogen bonding distance of S2B, could be a proton donor for some reactions of nitrogenase.[4] A considerable body of reactivity data for proteins modified at residue 195 has been considered in terms of this possible protonation capability.[73-76] However it is not clear how more than one proton could be delivered from 195^{His}, because a straightforward mechanism for replenishment of this proton on 195^{His} is not evident, and disruptive full rotation of the imidazole ring would be required.[17]

Homocitrate. At this point it is prudent to review the experimental data for proteins that substitute other di- and tri-carboxylic acids for homocitrate, since homocitrate is a key facilitator of the proposed mechanism. Many isomeric and similar hydroxy-carboxylic acids were tested as substitutes for homocitrate, by measurement of activities for reduction of N_2, C_2H_2 and H^+.[77,78] With the exception of *erythro*-1-fluorohomocitrate which retains the required structural elements of physiological homocitrate, all substitutes demonstrated severely diminished or undetectable ability to reduce N_2. Some substitutes (citrate, *R*-citramalate, *cis*-aconitate, 1-fluorohomocitrate) retained 50 - 70% of wild-type C_2H_2 reduction activity, and a larger number of homocitrate analogues demonstrated only partially diminished activity for proton reduction. Results for citrate, which cannot present the $CH_2CH_2COO^-$ arm containing O3 (Fig 3), are informative, because the crystal structure of the mutant $NifV^-$ Kp1 protein of *K. pneumoniae* containing citrate rather than homocitrate has been determined. This structure (PDB 1H1L) contains ambivalent density in the relevant domain around Mo, best modelled as part occupancy by citrate and part occupancy by water.[79] The citrate structure retains the equivalents of homocitrate O5 and O6. The water-chain W1 to W8 is intact in 1H1L, and there is a hydrogen bonding connection from W4 to the citrate carboxylate proxy of O3. Because the citrate arm containing this carboxylate is one CH_2 shorter than that in homocitrate, this W4--citrate hydrogen bond is longer (3.5Å) than W4--O3 (2.9Å). This is consistent with operation of the proton translocation mechanism with diminished efficacy in the citrate mutant, and the observed diminished ability to reduced C_2H_2. It is significant that the degree of diminution of activity in the mutant proteins[77,78] correlates with the number of protons required for the reaction (6 for N_2 > 2 for C_2H_2 and H^+), and with the difficulty of substrate reduction ($N_2 > C_2H_2 > H^+$). My conclusion for wild-type nitrogenase is that the proton translocation mechanism detailed here is obligatory for the reduction of N_2 and other substrates that require serial supply of multiple protons, whereas alternative proton supply routes could be sufficient for substrates requiring only two protons per reduction cycle.

Protein dynamics. How can the proposed mechanism for serial proton supply be further developed? The model calculated here has allowed some flexibility in the residues surrounding the water chain, but larger motions, and probably concerted movements, could be expected. In addition, the proposed proton translocation mechanism is yet linked to other mechanistic events in the reaction of nitrogenase – events such as N_2 ingress and binding, the operation of the Fe protein cycle and electron transfer to the P-cluster and to FeMo-co, and modification of the shape of FeMo-co as N_2 is hydrogenated to NH_3 on its surface. These observations point to the next objective, to understand larger scale conformational changes in the nitrogenase proteins, the character of the allostery in the full mechanism, and the low frequency dynamics of the MoFe nitrogenase protein.[80,81] All-atom molecular dynamics investigations of nitrogenase have been reported, with the specific objectives of identifying substrate or inhibitor transport pathways.[59,82] An alternative approach uses elastic network models (ENM) and normal mode analysis of coarse-grained structural models of the protein and cofactors.[83-86] This method captures large-scale collective structural motions, and the correlations of these motions for structural and functional elements of the protein, on relatively slow biologically-relevant time scales beyond the range of conventional molecular dynamics.[87,88]

Experiments involving modification of targeted residues to test this mechanism for proton transfer were discussed in the previous paper.[17]

Extensions. The results here provide an elaborate quantum calculation of the bond-making and bond-breaking steps for the Grotthuss mechanism of proton translocation, within an actual protein structure, with more detail than previously available. The potential energy surface mapping provides information about the distinctive geometry and energy changes for the slide and rotation steps involved. It has been sometimes thought that the rotation component would incur a substantial energy penalty,[28] but this is not so, because the barrier is effectively just that of breaking a single OH--O hydrogen bond. Further, the distinctive characteristic of the slide step is seen to be a very short O-H-O hydrogen bond, in the realm of such bonds that have been widely investigated as low-barrier-hydrogen-bonds.[89-93] Also revealed here is the rippling character of the water-water separations, between extremes of 2.45 and 3.5Å, as the slides (H_3O^+) and rotations progress along the chain.

These DFT-revealed bond making and breaking properties are not accessible via the parameterised molecular dynamics calculations of intra-protein water chains,[28,35] of which the proton pumping 'D pathway' in cytochrome c oxidase (CcO) is the most studied.[94,95] I have already described[17] the structural similarities between the water chain in nitrogenase and the D chain in CcO,[96-98] both of which translocate protons in one direction only (proton transfer in the 'K water chain' of CcO is different, being coupled with electron transfer and reduction of O_2[99,94,100]). The nitrogenase water path and the CcO D water chain contain similar numbers of water molecules, enclosed with strongly hydrogen bonding functions from the protein main-chain (O) and side-chains OH from tyrosine, serine, NH_2 from arginine, asparagine, carboxylate from aspartate: the main difference is the more frequent occurrence of main-chain N-H ••• water hydrogen bonds in the nitrogenase pathways. The present results for nitrogenase could assist in understanding the mechanism of Grotthuss proton-translocation through the D pathway of CcO, a process that has already been investigated using molecular dynamics.[101] In drosophilid alcohol dehydrogenases an eight-membered water chain apparently facilitates proton egress from active site to solvent.[102] I emphasise that the descriptions here for nitrogenase, and suggestions for CcO and related systems, concern only the *mechanism* of proton-translocation, not the thermodynamic factors controlling the direction of proton transfer.

Finally, some other related reports are noted, although none are comparable water chains. DFT calculations of small water aggregates mimicking carbonic anhydrase show comparable short hydrogen bonding distances and low proton transfer barriers.[103] Short hydrogen bonds engaged by a transferring proton were demonstrated in the QM/MM investigation of short distance proton transfer in an Fe_2 hydrogenase protein.[104] CTX-M Class A β-lactamase, hydrogen atoms in hydrogen bonds of 2.47Å and 2.53Å were detected by crystal diffraction, and the barrier for proton slide was calculated (QM/MM) to be 1.5 kcal mol^{-1}.[93]

Acknowledgments

This research is supported by UNSW Australia, and a grant from the Australian National Computational Infrastructure. Some molecular images were generated using CrystalMaker® (www.crystalmaker.com).

References

1 R. H. Burris, *J. Biol. Chem.*, 1991, **266**, 9339-9342.

2 J. W. Peters, K. Fisher and D. R. Dean, *Annu. Rev. Microbiol.*, 1995, **49**, 335-366.

3 B. K. Burgess and D. J. Lowe, *Chem. Rev.*, 1996, **96**, 2983-3011.

[4] J. B. Howard and D. C. Rees, *Chem. Rev.*, 1996, **96**, 2965-2982.

[5] J. Christiansen, D. R. Dean and L. C. Seefeldt, *Annu. Rev. Plant Physiol. Plant Mol. Biol.*, 2001, **52**, 269-295.

[6] R. Y. Igarashi and L. C. Seefeldt, *Crit. Rev. Biochem. Mol. Biol.*, 2003, **38**, 351-384.

[7] D. C. Rees, F. A. Tezcan, C. A. Haynes, M. Y. Walton, S. Andrade, O. Einsle and J. A. Howard, *Phil. Trans. Roy. Soc. A*, 2005, **363**, 971-984.

[8] J. B. Howard and D. C. Rees, *Proc. Nat. Acad. Sci. USA*, 2006, **103**, 17119-17124.

[9] L. C. Seefeldt, B. M. Hoffman and D. R. Dean, *Annu. Rev. Biochem.*, 2009, **78**, 701-722.

[10] C. H. Lee, Y. Hu and M. W. Ribbe, *Science*, 2010, **329**, 642.

[11] Z.-Y. Yang, D. R. Dean and L. C. Seefeldt, *J. Biol. Chem.*, 2011, **286**, 19417-19421.

[12] Y. Hu, C. C. Lee and M. W. Ribbe, *Science*, 2011, **333**, 753-755.

[13] C. C. Lee, Y. Hu and M. W. Ribbe, *Angew. Chem. Int. Ed.*, 2011, **50**, 5545-5547.

[14] L. C. Seefeldt, Z.-Y. Yang, S. Duval and D. R. Dean, *Biochimica et Biophysica Acta (BBA) - Bioenergetics*, 2013, **1827**, 1102-1111.

[15] I. Dance, *Chem Commun (Camb)*, 2013, **49**, 10893-10907.

[16] J. G. Rebelein, Y. Hu and M. W. Ribbe, *Angewandte Chemie International Edition*, 2014, **53**, 11543-11546.

[17] I. Dance, *Dalton Trans.*, 2012, **41**, 7647-7659.

[18] M. C. Durrant, *Biochem. J.*, 2001, **355**, 569-576.

[19] B. M. Barney, M. G. Yurth, P. C. Dos Santos, D. R. Dean and L. C. Seefeldt, *J. Biol. Inorg. Chem.*, 2009, **14**, 1015-1022.

[20] L. C. Seefeldt and D. R. Dean, *Acc. Chem. Res.*, 1997, **30**, 260-266.

[21] O. Einsle, *Journal of Biological Inorganic Chemistry*, 2014, **19**, 737-745.

[22] T. Spatzal, *Zeitschrift für anorganische und allgemeine Chemie*, 2015, **641**, 10-17.

[23] L.-M. Zhang, C. N. Morrison, J. T. Kaiser and D. C. Rees, *Acta Crystallographica Section D*, 2015, **71**, 274-282.

[24] C. N. Morrison, J. A. Hoy, L. Zhang, O. Einsle and D. C. Rees, *Biochemistry*, 2015, **54**, 2052-2060.

[25] I. Dance, *Sci Rep*, 2013, **3**, 3237.

[26] J. B. Howard, K. J. Kechris, D. C. Rees and A. N. Glazer, *PLoS One*, 2013, **8**.

[27] C. J. T. de Grotthuss, *Ann. Chim. (Paris)*, 1806, **58**, 54-74.

[28] S. Cukierman, *Biochimica et Biophysica Acta (BBA) - Bioenergetics*, 2006, **1757**, 876-885.

[29] N. Agmon, *Chemical Physics Letters*, 1995, **244**, 456-462.

[30] R. Pomès and B. Roux, *Biophys. J.*, 1998, **75**, 33-40.

[31] R. Pomès and B. Roux, *Biophysical Journal*, 2002, **82**, 2304-2316.

[32] P. Ball, *Chem. Rev.*, 2008, **108**, 74-108.

[33] C. Dellago, M. M. Naor and G. Hummer, *Phys. Rev. Lett.*, 2003, **90**, 105902.

[34] R. J. P. Williams, *J. Theoretical Biology*, 2002, **219**, 389-396.

[35] C. A. Wraight, *Biochimica et Biophysica Acta (BBA) - Bioenergetics*, 2006, **1757**, 886-912.

[36] I. Dance, *Inorg. Chem.*, 2006, **45**, 5084-5091.

[37] I. Dance, *Dalton Trans.*, 2012, **41**, 4859-4865.

[38] B. Delley, *J. Chem. Phys.*, 1990, **92**, 508-517.

[39] B. Delley, in *Modern density functional theory: a tool for chemistry*, eds. J. M. Seminario and P. Politzer, Elsevier, Amsterdam, 1995, p. 221-254

[40] J. Baker, A. Kessi and B. Delley, *The Journal of Chemical Physics*, 1996, **105**, 192-212.

[41] B. Delley, *J. Chem. Phys.*, 2000, **113**, 7756-7764.

[42] J. Andzelm, R. D. King-Smith and G. Fitzgerald, *Chemical Physics Letters*, 2001, **335**, 321-326.

[43] A. D. Becke, *Phys. Rev. A*, 1988, **38**, 3098-3100.

[44] C. Lee, W. Yang and R. G. Parr, *Phys. Rev. B*, 1988, **37**, 785-789.

[45] A. Klamt and G. Schüürmann, *J. Chem.Soc., Perkin Trans. 2*, 1993, 799-805.

[46] J. Andzelm, C. Kolmel and A. Klamt, *J. Chem. Phys.*, 1995, **103**, 9312-9320.

[47] B. Delley, *Molecular Simulation*, 2006, **32**, 117-123.

[48] I. G. Dance, in *Transition Metal Sulfur Chemistry: Biological and Industrial Significance*, eds. E. I. Stiefel and K. Matsumoto, American Chemical Society, Washington, DC, USA, 1996, p. 135-152

[49] I. Dance, *J. Chem. Soc., Chem. Commun.*, 1998, 523-530.

[50] Z. X. Cao, X. Jin and Q. N. Zhang, *Journal of Theoretical and Computational Chemistry*, 2005, **4**, 593-602.

[51] I. Dance, *Inorg. Chem.*, 2011, **50**, 178-192.

[52] C. Bianchini, D. Masi, M. Peruzzini, M. Casarin, C. Maccato and G. A. Rizzi, *Inorg. Chem.*, 1997, **36**, 1061-1069.

[53] I. Dance, *J. Am. Chem. Soc.*, 2005, **127**, 10925-10942.

[54] I. Dance, *J. Am. Chem. Soc.*, 2007, **129**, 1076-1088.

[55] P. E. M. Siegbahn, J. Westerberg, M. Svensson and R. H. Crabtree, *J. Phys. Chem. B*, 1998, **102**, 1615-1623.

[56] M. W. Chase, *J. Phys. Chem. Ref. Data*, 1998, **9**, 1-1951.

[57] I. Dance, *Molecular Simulation*, 2008, **34**, 923-929.

[58] I. Dance, *Molecular Simulation*, 2011, **37**, 257.

[59] D. Smith, K. Danyal, S. Raugei and L. C. Seefeldt, *Biochemistry*, 2014, **53**, 2278-2285.

[60] C. Ceccarelli, G. A. Jeffrey and R. Taylor, *Journal of Molecular Structure*, 1981, **70**, 255-271.

[61] G. A. Jeffrey and W. Saenger, 'Hydrogen Bonding in Biological Structures', Springer-Verlag, Berlin, New York, 1991.

[62] M. W. Feyereisen, D. Feller and D. A. Dixon, *The Journal of Physical Chemistry*, 1996, **100**, 2993-2997.

[63] G. R. Desiraju and T. Steiner, 'The Weak Hydrogen Bond in Structural Chemistry and Biology', Oxford University Press/International Union of Crystallography, Oxford, 1999.

[64] W. C. Hamilton and J. A. Ibers, 'Hydrogen bonding in solids', W. A. Benjamin, New York, 1968.

[65] B. S. Avvaru, C. U. Kim, K. H. Sippel, S. M. Gruner, M. Agbandje-McKenna, D. N. Silverman and R. McKenna, *Biochemistry*, 2010, **49**, 249-251.

[66] L. Noodleman and D. A. Case, *Adv. Inorg. Chem.*, 1992, **38**, 424-471.

[67] H. Beinert, *Journal of Biological Inorganic Chemistry*, 2000, **5**, 2-15.

[68] I. Dance and R. A. Henderson, *Dalton Transactions*, 2014, **43**, 16213-16226.

[69] I. Dance, *Dalton Trans.*, 2015, **44**, 4707-4717.

[70] I. Dance, *Inorg Chem*, 2013, **52**, 13068-13077.

[71] I. Dance, *Dalton Transactions*, 2015, **44**, 9027-9037.

[72] Z.-Y. Yang, K. Danyal and L. C. Seefeldt, *Methods Mol. Biol.*, 2011, **766**, 9-29.

[73] M. J. Dilworth, K. Fisher, C. H. Kim and W. E. Newton, *Biochemistry*, 1998, **37**, 17495-17505.

[74] K. Fisher, M. J. Dilworth and W. E. Newton, *Biochemistry*, 2000, **39**, 15570-15577.

[75] K. Fisher, M. J. Dilworth, C.-H. Kim and W. E. Newton, *Biochemistry*, 2000, **39**, 10855-10865.

[76] B. M. Barney, M. Laryukhin, R. Y. Igarashi, H.-I. Lee, P. C. Dos Santos, T.-C. Yang, B. M. Hoffman, D. R. Dean and L. C. Seefeldt, *Biochemistry*, 2005, **44**, 8030-8037.

[77] J. Imperial, T. R. Hoover, M. S. Madden, P. W. Ludden and V. K. Shah, *Biochemistry*, 1989, **28**, 7796-7799.

[78] M. S. Madden, N. D. Kindon, P. W. Ludden and V. K. Shah, *Proc. Nat. Acad. Sci. USA*, 1990, **87**, 6517-6521.

[79] S. M. Mayer, C. A. Gormal, B. E. Smith and D. M. Lawson, *J. Biol. Chem.*, 2002, **277**, 35263-35268.

[80] I. Bahar, C. Chennubhotla and D. Tobi, *Current Opinion in Structural Biology*, 2007, **17**, 633-640.

[81] I. Balabin, W. Yang and D. N. Beratan, *Proc. Nat. Acad. Sci. USA*, 2009, **106**, 14253-14258.

[82] L. B. Gee, I. Leontyev, A. Stuchebrukhov, A. D. Scott, V. Pelmenschikov and S. P. Cramer, *Biochemistry*, 2015, **54**, 3314-3319.

[83] M. Tirion, *Phys. Rev. Lett.*, 1996, **77**, 1905-1908.

[84] A. R. Atilgan, S. R. Durell, R. L. Jernigan, M. C. Demirel, O. Keskin and I. Bahar, *Biophysical Journal*, 2001, **80**, 505-515.

[85] F. Tama and Y.-H. Sanejouand, *Protein Eng.*, 2001, **14**, 1-6.

[86] I. Balabin, D. N. Beratan and I. Dance, *unpublished work*, 2008.

[87] I. Bahar and A. J. Rader, *Current Opinion in Structural Biology*, 2005, **15**, 586-592.

[88] F. Tama and C. L. Brooks, *Annual Review of Biophysics and Biomolecular Structure*, 2006, **35**, 115-133.

[89] W. W. Cleland, *Archives of Biochemistry and Biophysics*, 2000, **382**, 1-5.

[90] C. L. Perrin, *Accounts of Chemical Research*, 2010, **43**, 1550-1557.

[91] R. Chaudret, G. A. Cisneros, O. Parisel and J.-P. Piquemal, *Chemistry – A European Journal*, 2011, **17**, 2833-2837.

[92] Y. Ogata, M. Daido, Y. Kawashima and M. Tachikawa, *RSC Advances*, 2013, **3**, 25252-25257.

[93] D. A. Nichols, J. C. Hargis, R. Sanishvili, P. Jaishankar, K. Defrees, E. W. Smith, K. K. Wang, F. Prati, A. R. Renslo, H. L. Woodcock and Y. Chen, *Journal of the American Chemical Society*, 2015, **137**, 8086-8095.

[94] P. E. M. Siegbahn and M. R. A. Blomberg, *Chem. Rev.*, 2010, **110**, 7040-7061.

[95] M. Wikstrom and M. I. Verkhovsky, *Biochimica et Biophysica Acta -Bioenergetics*, 2011, **1807**, 1273-1278.

[96] L. Qin, C. Hiser, A. Mulichak, R. M. Garavito and S. Ferguson-Miller, *Proc. Nat. Acad. Sci. USA*, 2006, **103**, 16117-16122.

[97] L. Qin, J. Liu, D. A. Mills, D. A. Proshlyakov, C. Hiser and S. Ferguson-Miller, *Biochemistry*, 2009, **48**, 5121-5130.

[98] J. Liu, L. Qin and S. Ferguson-Miller, *Proc. Nat. Acad. Sci. USA*, 2011, **108**, 1284-1289.

[99] V. R. I. Kaila, M. I. Verkhovsky and M. Wikstrom, *Chemical Reviews*, 2010, **110**, 7062-7081.

[100] T. Tiefenbrunn, W. Liu, Y. Chen, V. Katritch, C. D. Stout, J. A. Fee and V. Cherezov, *PLoS ONE*, 2011, **6**, e22348.

[101] J. Xu and G. A. Voth, *Proc. Nat. Acad. Sci. USA*, 2005, **102**, 6795-6800.

[102] Y. Wuxiuer, E. Morgunova, N. Cols, A. Popov, A. Karshikoff, I. Sylte, R. Gonzàlez-Duarte, R. Ladenstein and J.-O. Winberg, *FEBS Journal*, 2012, **279**, 2940-2956.

[103] Q. Cui and M. Karplus, *The Journal of Physical Chemistry B*, 2003, **107**, 1071-1078.

[104] G. Hong, A. J. Cornish, E. L. Hegg and R. Pachter, *Biochim. Biophys. Acta Bioenergetics*, 2011, **1807**, 510-517.

The pathway for serial proton supply to the active site of nitrogenase: enhanced density functional modeling of the Grotthuss mechanism

Ian Dance

School of Chemistry, UNSW Australia, Sydney 2052, Australia

Contents graphic and text

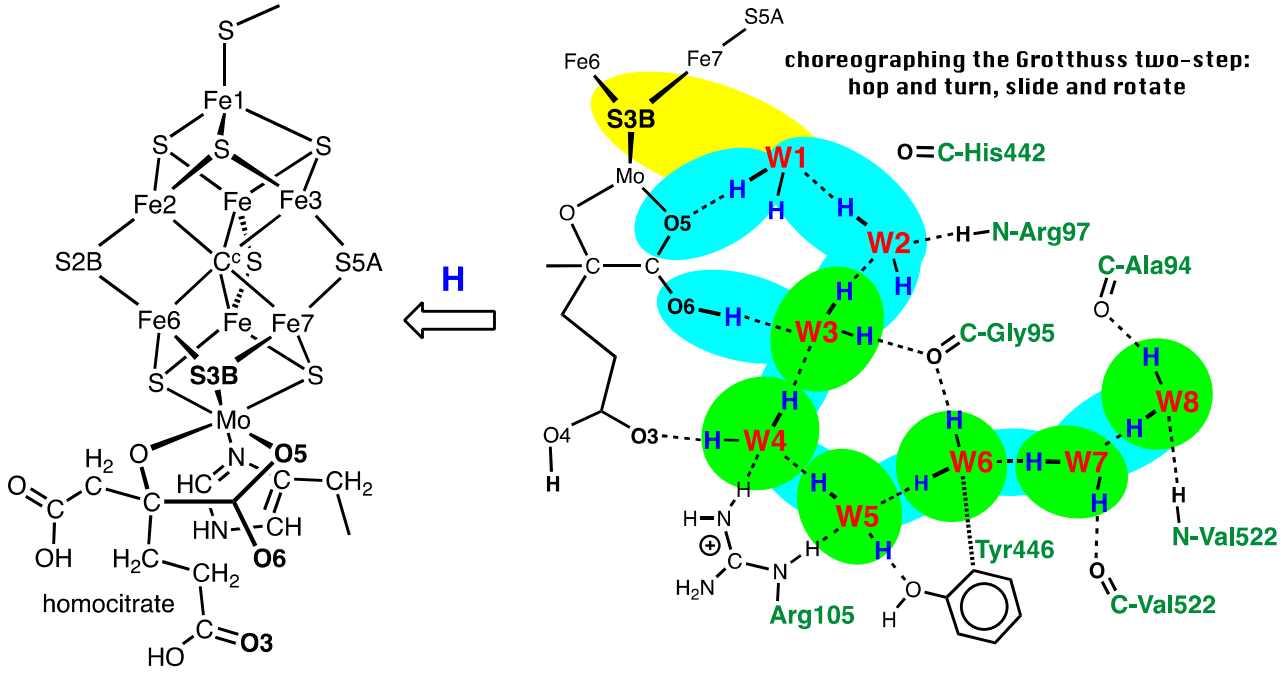

Proton translocation along a chain of eight waters to the active site of nitrogenase is described in detail, using density functional simulations with a 269 atom system that includes surrounding amino acids.